

## SEYFERT GALAXIES: NUCLEAR RADIO STRUCTURE AND UNIFICATION

DHARAM V. LAL<sup>1,2,3</sup>, PRAJVAL SHASTRI<sup>1</sup>, DENISE C. GABUZDA<sup>4</sup>

<sup>1</sup>Indian Institute of Astrophysics, Koramangala, Bangalore 560034, India

<sup>2</sup>Joint Astronomy Programme, Department of Physics, Indian Institute of Science, Bangalore 560012, India

<sup>3</sup>Harvard-Smithsonian Center for Astrophysics, 60 Garden Street, Cambridge, MA 02138, USA and

<sup>4</sup>Department of Physics, University College Cork, Cork, Republic of Ireland

*Accepted for publication in The Astrophysical Journal, Issue 730–2*

### ABSTRACT

A radio study of a carefully selected sample of 20 Seyfert galaxies that are matched in orientation-independent parameters, which are measures of intrinsic active galactic nuclei (AGN) power and host galaxy properties is presented to test the predictions of the unified scheme hypothesis. Our sample sources have core flux densities greater than 8 mJy at 5 GHz on arcsec-scales due to the feasibility requirements. These simultaneous pc-scale and kpc-scale radio observations reveal (i) that Seyfert 1 and Seyfert 2 galaxies have equal tendency to show compact radio structures on mas-scales, (ii) the distributions of pc-scale and kpc-scale radio luminosities are similar for both Seyfert 1 and Seyfert 2 galaxies, (iii) no evidence for relativistic beaming in Seyfert galaxies, (iv) similar distributions of source spectral indices in spite of the fact that Seyferts show nuclear radio flux density variations, and (v) the distributions of projected linear size for Seyfert 1 and Seyfert 2 galaxies are not significantly different as would be expected in the unified scheme. The latter could be mainly due to a relatively large spread in the intrinsic sizes. We also find that a starburst alone cannot power these radio sources. Finally, an analysis of the kpc-scale radio properties of the CfA Seyfert galaxy sample shows results consistent with the predictions of the unified scheme.

*Subject headings:* Galaxies: Seyfert – Radio continuum: galaxies

### 1. INTRODUCTION

Active galaxies are classified according to their appearance, luminosity, and spectra into the following principal types: Seyfert galaxies, radio galaxies, quasars, and BL Lacertae objects. Khachikian & Weedman (1974) identified two types of Seyfert galaxies on the basis of the widths of the nuclear emission lines. While spectra of type 2 Seyfert galaxies have a single set of relatively narrow emission lines (whose width can be characterized in terms of full width at half maximum,  $\text{FWHM} \approx 300\text{--}1,000 \text{ km s}^{-1}$ ), the spectra of type 1 Seyfert galaxies have an additional much broader component ( $\text{FWHM} \geq 1,000 \text{ km s}^{-1}$ ) of hydrogen and helium lines. In the simplest cases, the broad component is either absent (Seyfert 2) or strong and dominant (Seyfert 1). With better data, it became clear that there is a wide range in the relative strength of the broad and narrow emission lines, and this led to refinement of the Seyfert classification by introducing intermediate types (Osterbrock 1981; Osterbrock & Pogge 1985). As the broad component of  $\text{H}\beta$  becomes weaker relative to the narrower component, the Seyfert type changes from 1 to 1.2 to 1.5 to 1.8. For Seyfert 1.8 galaxies, weak broad wings are just visible at the base of  $\text{H}\beta$ , while in Seyfert 1.9 galaxies they are only visible on the  $\text{H}\alpha$  emission line at 6563 Å. In practice, these Seyfert sub-types have not been formally defined but instead give an overall indication of the degree to which the broad component is present.

The technique of spectropolarimetry yielded spectra that showed broad lines in polarized light in Seyfert 2 galaxies. This polarized light was interpreted to be the light that was initially moving out of the nucleus in one direction which was then reflected into our line of sight. Such a technique could detect broad line regions (BLRs) in a Seyfert 2 galaxy, *e.g.* NGC 1068 (Miller & Goodrich 1990). This led to the unified scheme model (Antonucci 1993; Lawrence & Elvis

2010), which is the key idea being used to organize and make sense of our large and growing observational information about Seyfert galaxies, *i.e.* Seyfert 2 galaxies are intrinsically Seyfert 1 galaxies whose continuum and broad-line emission is attenuated in the direction of the observer.

Several investigations in the literature have yielded results consistent with the predictions of this scheme, *e.g.*, the featureless continuum is stronger in Seyfert 1 than in Seyfert 2 galaxies (Lawrence 1987; Mas-Hesse et al. 1994). Kinney et al. (1991) showed similar ultraviolet slopes for Seyfert 2 and Seyfert 1 galaxies. The active galactic nucleus (AGN) of Seyfert 2 galaxy is clearly seen in  $\text{H}\alpha$ , but is barely detected in the ultraviolet images (Colina et al. 1997). The ionizing radiation is roughly collimated before emerging into the narrow line region perhaps due to an obscuring torus (Whittle et al. 1988) and is sometimes cone-shaped (Pogge 1989; Evans et al. 1991A,B, 1993, 1994), which appear smaller in Seyfert 1 than Seyfert 2 galaxies (Kriss et al. 1994; Mulchaey, Wilson, & Tsvetanov 1996; Colina et al. 1997; Heckman et al. 1997; Muñoz Marín et al. 2007; González-Delgado et al. 1998). Furthermore, for a given far-infrared luminosity, Lawrence & Elvis (1982) found a significant lack of soft X-ray emission in Seyfert 2 galaxies compared to Seyfert 1 galaxies (see also Mas-Hesse et al. 1994; Cappi et al. 1996) and Mas-Hesse et al. (1994) found similar distributions of the hard X-ray emission for both kinds of Seyfert galaxies. Maiolino et al. (1997) and Curran (2000) found no differences in the mean ratio of CO and far-infrared luminosity between the two Seyfert classes suggesting that both Seyfert types have the same amount of molecular gas. Morganti et al. (1999) found that Seyfert 2 galaxies tend to have a larger projected radio linear size than Seyfert 1 galaxies, whereas there is no statistically significant difference in radio power between Seyfert 1 and Seyfert 2 galaxies. Recently, Gallimore et al. (2010) found that Seyfert 1's show

silicate emission on average and Seyfert 2's show silicate absorption, which is broadly compatible with the obscuring torus interpretation. While the unified scheme is simple and attractive, there are some observational results that are inconsistent with it, such as, the presence of relatively young ( $\sim 1$  Gyr) stellar populations in Seyfert 2 galaxies (Schmitt et al. 1999; González-Delgado et al. 2001; Raimann et al. 2003); Malkan, Gorjian, & Tam (1998) found that Seyfert 2 galaxies, on average, tend to have later morphological types than the Seyfert 1 galaxies; Dultzin-Hacyan et al. (1999) confirmed that Seyfert 2 galaxies have an excess of nearby companions over Seyfert 1 galaxies; the scattered BLR is not detected in many Seyfert 2 galaxies (Tran 2001, 2003); a lack of X-ray absorption in several Seyfert 2 galaxies (Panessa & Bassani 2002); Seyfert 2s having a higher propensity for nuclear starbursts (Buchanan et al. 2006); and Roy et al. (1994) found a lower detection rate of compact radio cores in Seyfert 1 than Seyfert 2 galaxies.

It was Roy et al.'s (1994) observational result which prompted us to commence this study. In the unified scheme, since the torus is expected to be transparent to emission at radio wavelengths, the compact features should be similarly visible in Seyfert 1 and Seyfert 2 galaxies. Further, the inconsistency with the unification scheme cannot be eased by invoking relativistic beaming, because then, the face-on AGNs, *viz.*, Seyfert 1 galaxies, would be more likely to show compact structures. We aimed to rigorously test the predictions of the unified scheme by investigating the compact radio morphology of Seyfert galaxies. To achieve this goal, we constructed a sample of Seyfert 1 and Seyfert 2 galaxies that are matched in orientation-independent parameters, which are measures of intrinsic AGN power and host galaxy properties.

In this paper we first describe the construction of the sample (Section 2) and use the radio maps for 15 objects presented in our earlier paper (Lal, Shastri, & Gabuzda 2004) along with previously published data for the remaining five objects to interpret our results and their implications on the unification scheme hypothesis (Section 3). In Section 3.7 we also interpret the results of arcsec-scale radio observations of Kukula et al. (1995) for the CfA Seyfert galaxy sample (Huchra & Burg 1992) and their implications on the unification scheme hypothesis. Finally, we summarize our conclusions in Section 4.

Throughout the paper we use the terms “pc-scale” and “kpc-scale” interchangeably for “mas-scale” and “arcsec-scale”, respectively. We also use “face-on” and “edge-on” interchangeably for “Seyfert 1” and “Seyfert 2” galaxies, respectively. We assume a cosmology with  $H_0 = 75 \text{ km s}^{-1} \text{ Mpc}^{-1}$  and  $q_0 = 0$ . We define the spectral index  $\alpha$  in the sense that  $S_\nu \propto \nu^{-\alpha}$ , where  $S_\nu$  and  $\nu$  are flux density and frequency, respectively. Since, we are dealing with small number statistics, we use Mann-Whitney U test<sup>1</sup> (Siegel & Castellan 1981) to test the null hypothesis.

<sup>1</sup> Mann-Whitney U test is a non-parametric statistical hypothesis test for small sample sizes,  $\lesssim 20$  (Siegel & Castellan 1981). It analyzes the degree of separation (or the amount of overlap) between the two groups. For example, the null hypothesis assumes that the two Seyfert sub-sample types are homogeneous and come from the same population (significance level, say  $\lesssim 0.05$ ). The test involves the calculation of a statistic, called U, whose distribution under the null hypothesis is known. Significance is verified by using the computed test statistic (e.g., U) and comparing this statistic (probability value) with the Null Hypothesis value ( $\lesssim 0.05$ ). If the former exceeds the latter, there is certainly sufficient evidence to accept the Null Hypothesis. For large samples, U is approximately normally distributed.

## 2. SAMPLE

The differences observed in samples of Seyfert galaxies can be explained by the selection techniques used for assembling them. For example, in the Markarian Survey, spectroscopic investigations have shown that  $\sim 10\%$  of all discovered 1500 galaxies with a strong ultraviolet continuum are Seyfert galaxies (Markarian 1967; Markarian et al. 1986). Therefore, such a sample suffers from deficiency of Seyfert 2 galaxies, which is most probably a result of the survey selection effect. This is due to the fact that Seyfert 2 galaxies do not have excessive ultraviolet continua due to obscuration and thus could easily elude the ultraviolet search method (Meurs & Wilson 1984). The CfA Seyfert galaxy sample is the first of the optically selected complete samples with spectroscopic identifications and is due to Huchra & Burg (1992). The sample has an equal number of Seyfert 1 and Seyfert 2 galaxies (25 & 23 respectively). The unresolved optical nucleus of a Seyfert grows fainter with the square of distance, whilst the surface brightness of its host galaxy remains constant over a constant aperture. Therefore, in this sample the ratio of the two components, the host galaxy surface brightness to the active nucleus surface brightness, is highly variable. Ho & Ulvestad (2001) have discussed that the optical and ultraviolet selected samples are likely to have inherent biases against the obscured sources. Similarly, the IRAS survey would most probably detect reddened Seyfert 1 galaxies, but it may not be easy to isolate them from the much more luminous starburst galaxies (Heckman 1990A,B; Ho & Ulvestad 2001; Buchanan et al. 2006). In other words, the Seyfert samples based on the IRAS survey would be contaminated due to the presence of luminous starburst galaxies. Soft X-ray surveys may contain a larger fraction of soft X-ray Seyfert 1 galaxies, since Seyfert 2 galaxies are weak soft X-ray sources (Veron 1986; Lawrence & Elvis 2010). It therefore seems that most of the Seyfert galaxy samples (optical, infrared, and/or X-ray) have their biases and hence do not provide a good platform to test the unification scheme hypothesis. A Seyfert sample selected based on the orientation-independent parameters, which are measures of AGN power and host galaxy properties, would provide a good platform to test the predictions of the unification scheme hypothesis.

### 2.1. *Bona fide Seyfert galaxies*

The similarities between the nuclei of Seyfert galaxies and QSOs have often been pointed out (Seyfert and starburst galaxies: Dahari & De Robertis (1988); low-ionization nuclear emission line regions (LINERs) and radio-quiet quasars: Ho & Ulvestad (2001), Falcke et al. (2000), Ho et al. (1997); Low-Luminosity AGN: Nagar et al. (2000); etc.), and numerous efforts have been made to demonstrate a continuity between these objects. Any Seyfert sample is rarely ever free from starburst galaxies, LINERs, radio-quiet quasars, or radio-loud objects (Kauffmann et al. 2003A,B; Krongold et al. 2002; Levenson et al. 2001; Storchi-Bergmann et al. 2001; Hunt & Malkan 1999). Thus, we require the Seyfert galaxies that we select satisfy the following definition:

- Its host is a spiral galaxy (Weedman 1977) of Hubble type S0 or later (*i.e.* S0, Sa, Sab, Sb, Sbc, and Sc) (Sandage 1975). Radio-loud AGNs tend to reside in elliptical host galaxies (Urry & Padovani 1995), and radio-quiet AGNs inhabit mostly spiral galaxies. Thus we avoid any confusion due to the dichotomy of

host-galaxy type which may be linked with the radio-loud/radio-quiet dichotomy.

- Objects have low optical luminosity,  $M_B \geq -23$ , in order to avoid radio-quiet quasars (Schmidt & Green 1983).
- It is a radio-quiet object, *i.e.* the ratio of 5 GHz to B-Band flux density is less than 10 (Kellermann et al. 1989).
- The nuclear line width of permitted line,  $H\beta_{FWHM}$  (or  $H\alpha_{FWHM}$ ), is more than 1,000 km s<sup>-1</sup> (Khachikian & Weedman 1974) for Seyfert 1 galaxies, and line intensity ratio of [O III]  $\lambda 5007$  to  $H\beta$  is greater than three for Seyfert 2 galaxies (Dahari & De Robertis 1988). LINERs (or H II region) galaxies occasionally show nuclear  $H\beta_{FWHM}$  (or  $H\alpha_{FWHM}$ ) line width more than 1,000 km s<sup>-1</sup> (Ho & Ulvestad 2001; Ho et al. 1997; Peterson 1997, p. 24), but such galaxies never show line intensity ratio of [O III]  $\lambda 5007$  to  $H\beta$  greater than three (Ho, Filippenko, & Sargent 1996; Krolik 1999, p. 318). Or in other words, LINERs have a characteristically lower ionization state than Seyfert nuclei. Thus, we attempt to avoid any likely contamination due to the presence of LINERs and H II region galaxies in our Seyfert sample.

## 2.2. Criteria for the feasibility of our experiment

The sensitivity of an array is defined by the System Equivalent Flux Density (*SEFD*) (Wrobel 1995, 2000). The root-mean-square (RMS) thermal noise  $\Delta S$  in the visibility amplitude of a single polarization baseline between antennas  $i$  and  $j$  is

$$\Delta S = \frac{1}{\eta_S} \times \frac{\sqrt{SEFD_i \times SEFD_j}}{\sqrt{2 \times \Delta\nu \times \tau}} \text{ Jy}$$

(Wrobel 1995, 2000), where  $\eta_S \leq 1$  accounts for the very-long-baseline-interferometry (VLBI) system inefficiency;  $\tau$  is the integration time (in seconds) for an individual scan, which should be less than or equal to the coherence time, and  $\Delta\nu$  is the bandwidth (Hz). Next, the RMS thermal noise  $\Delta I_m$ , expected in a single polarization image, assuming natural weighting (Wrobel 1995) is

$$\Delta I_m = \frac{1}{\eta_S} \times \frac{SEFD}{\sqrt{N \times (N-1) \times \Delta\nu \times t_{int}}} \text{ Jy beam}^{-1},$$

where  $N$  is the number of antennas used and  $t_{int}$  is the total integration time on source. For example, the RMS noise level  $\sigma$  on a baseline between two very-long-baseline-array (VLBA) antennas for a data rate of 128 Mbits s<sup>-1</sup>, 2 min scan integration time, and 6 cm observing wavelength is 4.7 mJy (Wrobel 2000). A signal of  $6\sigma$  (= 28.2 mJy) is required to ensure reliable detection of the correlated signal; *i.e.*, the minimum detectable correlated flux density on each baseline. We further adopted a scan integration time of 8.8 min, which does not exceed the expected coherence time at 6 cm. A single tape pass lasts 44 min; with a scan duration of 8.8 min, exactly five scans will fit in each tape pass. Increasing the scan integration time will decrease the detectable flux density on all baselines; also adding the sensitive Effelsberg and phased-very-large-array (phased-VLA) to the array will provide additionally reduced detectable flux densities on baselines involving these antennas. Hence, we decided to use 11 US

TABLE 1  
TABLE SHOWING  $6\sigma$  CORRELATED FLUX DENSITIES, MINIMUM RELIABLY DETECTABLE FLUX DENSITIES ON VARIOUS BASELINES FOR A DATA RATE OF 128 MBITS S<sup>-1</sup>, A SCAN INTEGRATION TIME OF 8.8 MIN, AND AN OBSERVING FREQUENCY OF 5 GHz.

Baseline	Correlated flux density
Phased-VLA and Effelsberg	~ 0.7 mJy
Phased-VLA and VLBA-station	~ 2.6 mJy
Effelsberg and VLBA-station	~ 3.4 mJy
VLBA-station and VLBA-station	~ 13.5 mJy

stations (10 VLBA antennas and the phased-VLA) and three European-VLBI-Network stations. Torun and Noto stations along with Effelsberg provided us with a closure triangle in Europe and gave a range of baseline lengths for the sensitive baselines involving Effelsberg antenna. Similarly VLBA stations spread all over the United States provided us with a range of baseline lengths for sensitive baselines involving phased-VLA. Table 1 gives  $6\sigma$  correlated flux densities, minimum reliably detectable flux densities on various baselines for a data rate of 128 Mbits s<sup>-1</sup>, a scan integration time of 8.8 min, and an observing frequency of 5 GHz. Finally, if we wish to have at least ~ 4 mJy of correlated flux density, corresponding to the  $6\sigma$  detection limits for baselines between one of the smaller antennas in the array and either the phased-VLA or Effelsberg, the flux density in compact arcsec-scale structure must be ~ 8 mJy, assuming that 50% of the flux density seen with arcsec-scale resolution would be detected with the above baselines.

Therefore, the following constraint was enforced for the feasibility requirements: The source must have been observed with at least arcsec-scale resolution, at wavelengths of 6 cm (*i.e.*, VLA A or B array observations at these wavelengths), and it must have a detected compact component with flux density greater than 8 mJy. For objects that do not have  $\lambda_{6 \text{ cm}}$  measurements, we used  $\lambda_{3.6 \text{ cm}}$  VLA A array flux densities and assumed a flat spectral index between these two wavelengths for these objects. This constraint provides us with a reasonable sample size with minimum correlated flux density that is detectable on baselines involving Effelsberg antenna or phased-VLA.

## 2.3. Criterion to minimize obscuration of optical properties

Next, we restrict our list of objects to those with a ratio of minor to major isophotal diameter axes of the host galaxies greater than half. We thereby exclude edge-on spiral hosts and hence try to minimize obscuration of optical properties due to transmission through an edge-on galactic disk. Figure 1A shows the distribution of the ratio of minor to major isophotal diameter axes,  $b/a$ , for the final list of objects for the two Seyfert sub-classes. The isophotal diameter ratios are gleaned from de Vaucouleurs et al. (1991) and Lipovetsky et al. (1988) catalogs. We note that Pringle et al. (1999); Schmitt et al. (2001) and Nagar & Wilson (1999) have shown that there is no correlation between the host galaxy rotation axis and the direction of the radio jet.

## 2.4. Criteria based on orientation-independent parameters

We discussed in Section 1 that Roy et al.'s (1994) result is inconsistent with the unified scheme hypothesis and the inconsistency is only made worse by invoking relativistic beaming. To rigorously test the predictions of the unified scheme,

the purportedly face-on and edge-on Seyfert galaxies being compared should be *intrinsically similar* within the framework of the scheme. They should therefore be selected so that they are matched in parameters that are orientation independent. We attempt to do this with orientation-independent parameters that are measures of intrinsic AGN power and host galaxy properties. Such a selection would enable us to test the predictions of the unified scheme hypothesis rigorously. Therefore, from the short list of objects that met the criteria given in Sections 2.1, 2.2, and 2.3, we chose 10 Seyfert 1 and 10 Seyfert 2 galaxies, i.e., two matched samples of Seyfert 1 and Seyfert 2 galaxies, such that these two matched samples had similar distributions of the following orientation-independent parameters.

#### 2.4.1. Heliocentric redshift

In order to compare the Seyfert 1 and Seyfert 2 galaxies from the same volume of space, we chose them to have similar distribution of redshift. Figure 1B shows the distribution of redshift,  $z$ , for the two Seyfert sub-classes.

#### 2.4.2. Luminosity of the [O III] $\lambda 5007$ emission line: Measure of intrinsic AGN power

It is well known that narrow-line luminosities, *e.g.*, the luminosity of the [O III]  $\lambda 5007$  emission line correlate strongly with nuclear ionizing luminosity (Nelson & Whittle 1995; Whittle 1992B,C; Yee 1980; Shuder 1981). Furthermore, although spatially it could be distributed anisotropically (Pogge 1989; Evans et al. 1991A,B) its luminosity is clearly orientation independent. We therefore use the [O III]  $\lambda 5007$  luminosity as a measure of the intrinsic AGN power (Nelson & Whittle 1995), and we chose only those Seyfert 1 and Seyfert 2 galaxies that had similar distribution of [O III]  $\lambda 5007$  luminosity. Figure 1C shows the distribution of [O III]  $\lambda 5007$  luminosity for the two Seyfert sub-classes.

#### 2.4.3. Stellar luminosity of the host galaxy

The host galaxy properties of Seyfert galaxies ought to be orientation independent within the unified scheme. Hence, we chose stellar luminosity of the host galaxy (total luminosity of the host corrected for the nuclear non-stellar and emission line flux, redshift (K) correction, the internal absorption, and the Galactic absorption) as one of the parameters. Most of our sample objects have stellar absolute magnitude of the host galaxy, *i.e.*,  $M_B^{\text{total}}$  tabulated in Whittle (1992A). To determine corrections to total apparent magnitude,  $B_T$  (for Mrk 1218, NGC 2639, and Mrk 231), for which  $M_B^{\text{total}}$  is not available in Whittle (1992A), we stick to the methodology of Whittle (1992A). Four factors, together called  $(\Delta m)^{\text{correction}}$ , contribute to  $B_T$ , the first is the nuclear non-stellar and emission line flux,  $\Delta m_A$ , the second is the redshift (K) correction,  $\Delta m_K$ , the third is the correction for internal absorption,  $\Delta m_i$ , and the fourth is the correction due to galactic absorption,  $\Delta m_G$ . Thus

$$B_T^c = B_T + (\Delta m)^{\text{correction}},$$

where

$$(\Delta m)^{\text{correction}} = \Delta m_A + \Delta m_K + \Delta m_i + \Delta m_G,$$

which typically is  $\lesssim 0.4$  (Whittle 1992A). The third reference catalogue of bright galaxies (RC3, de Vaucouleurs et al. 1991) catalog gives  $B_T^0$ , *i.e.* the  $B_T$  corrected for redshift (K)

correction, the correction for internal absorption, and the correction due to galactic absorption, *i.e.*

$$B_T^0 = B_T + \Delta m_K + \Delta m_i + \Delta m_G.$$

We then determine  $B_T^c$ , using

$$B_T^c = B_T^0 + \Delta m_A.$$

$\Delta m_A$ , correction due to the non-stellar line and continuum emission is derived from the two line fluxes  $F_{5007}$  and  $F_{H\beta}$ , following the procedure described in Whittle (1992A). If only one of  $F_{5007}$  or  $F_{H\beta}$  is available, as is the case for NGC 2639, the other is estimated using  $F_{5007}/F_{H\beta} = 0.25$  for a Seyfert 1.0. As a function of redshift,  $z$ , the effective continuum flux density,  $F_c$ ,

$$F_c = F_{cF} + F_{cH} + F_{cC},$$

in  $\text{ergs s}^{-1} \text{cm}^{-2} \text{\AA}^{-1}$  in the  $B$  band due to forbidden and Balmer emission lines is approximated by

$$F_{cF} \simeq (0.62 - 3.5z) F_{5007}/980 \quad (z \leq 0.02),$$

$$F_{cF} \simeq 0.55 F_{5007}/980 \quad (0.02 < z \leq 0.07),$$

$$F_{cH} \simeq 1.42 F_{H\beta}/980 \quad (z \leq 0.03),$$

$$F_{cH} \simeq (1.51 - 3.14z) F_{H\beta}/980 \quad (0.03 < z \leq 0.07).$$

The non-stellar continuum luminosity is derived from  $H\beta$ , assuming a power law with spectral index  $\alpha$  ( $F_\nu \propto \nu^\alpha$ ). The effective continuum flux density in the  $B$  Band is given by

$$F_{cC} \simeq 1.10^{(\alpha+2)} (1+z)^{(\alpha+2)} F_{H\beta}/100.$$

We adopt  $\alpha = -1.0$  for the non-stellar continuum since this corresponds to the canonical nuclear colors of Seyfert 1 galaxies ( $\alpha = -1.0$  is equivalent to  $U-B = -0.75$ ,  $B-V = +0.41$ ). The total non-stellar contribution gives

$$\Delta m_A = 2.5 \log\left(\frac{7.2 \times 10^{-9}}{F_c}\right),$$

which is subtracted from  $B_T^0$  to give  $B_T^c$  for Mrk 1218, NGC 2639, and Mrk 231.  $M_B^{\text{total}}$  of the host galaxy is then determined using

$$M_B^{\text{total}} = B_T^c - 5 \log_{10}\left(\frac{r}{10 \text{ (pc)}}\right),$$

where  $r$  is the distance to the object in parsec. Figure 1D shows the distribution of the total stellar absolute magnitude,  $M_B^{\text{total}}$ , for the two Seyfert sub-classes.

#### 2.4.4. Absolute bulge luminosity of the host galaxy

Whittle (1992A) has argued that the nuclear stellar velocity dispersion is a measure of the depth of the gravitational potential within a scale of  $\sim 3$  kpc. Further, dispersion velocity of stars correlates with the absolute bulge magnitude (Whittle 1992A; Nelson & Whittle 1995). We took this depth of gravitational potential, *i.e.* the absolute magnitude of the bulge  $M_B^{\text{bulge}}$ , to be an indicator of intrinsic AGN power. Once again, the determination of  $M_B^{\text{bulge}}$  was performed in the following manner:  $M_B^{\text{bulge}}$  is available for most of the objects in Whittle (1992A). For Mrk 1218, NGC 2639, Mrk 231, and Mrk 477, we use the formulation adopted by Whittle (1992A), *i.e.*

$$M_B^{\text{bulge}} = M_B^{\text{total}} - (\Delta m)_{\text{disk}},$$

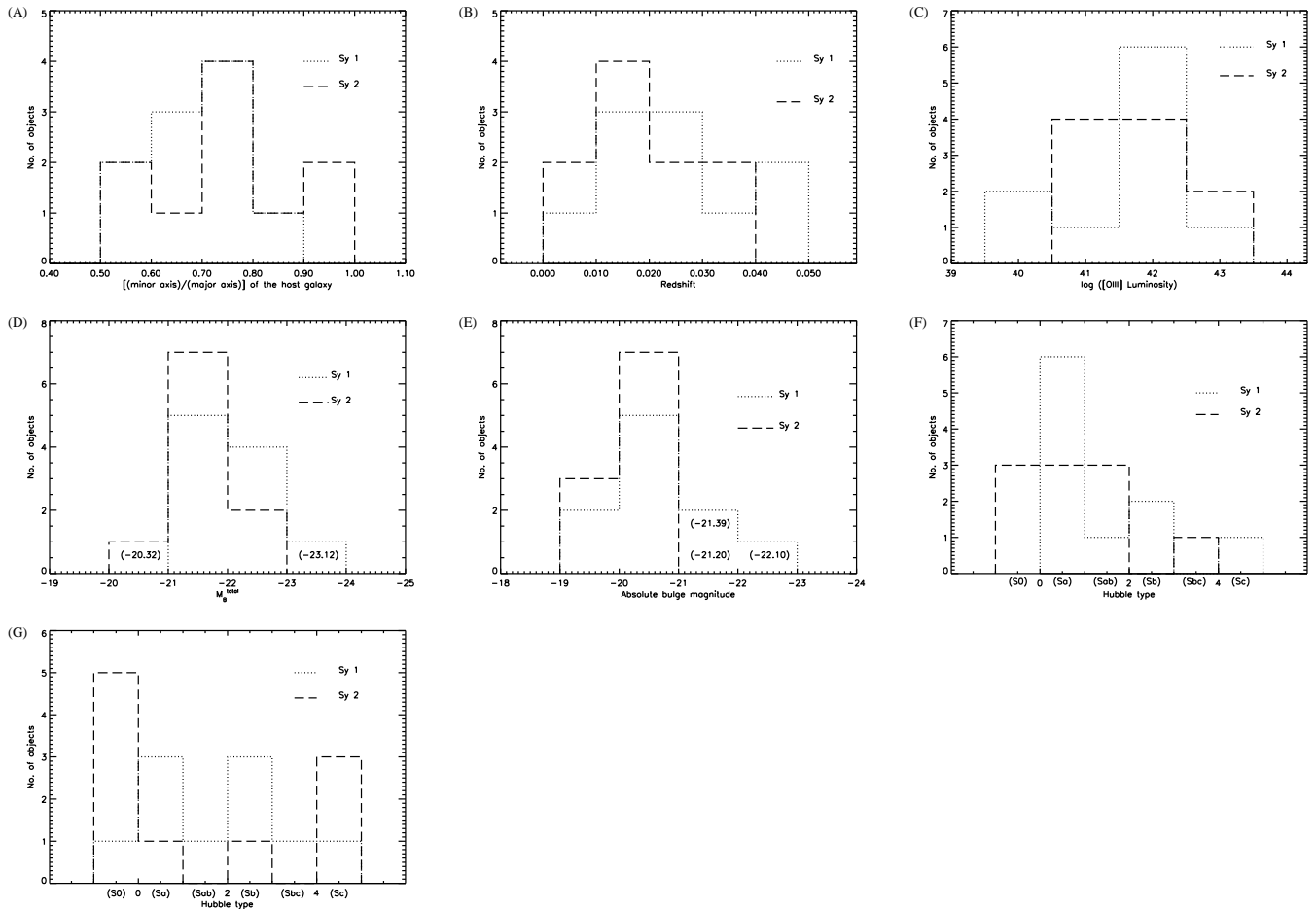


FIG. 1.— Histograms showing distributions of ratio of the minor to the major isophotal diameter axes,  $b/a$  (A), redshift,  $z$  (B),  $[O\ III]\ \lambda 5007$  luminosity (C), total stellar absolute magnitude of the host galaxy,  $M_B^{\text{total}}$  (D; values in the bin indicate  $M_B^{\text{total}}$  for the sources), absolute magnitude of the bulge ( $B$  band),  $M_B^{\text{bulge}}$  (E; values in the bin indicate  $M_B^{\text{bulge}}$  for the sources), the Hubble type,  $T$  (F; mainly gleaned from RC3 catalog, or Whittle 1992A, or Lipovetsky et al. 1988), and the Hubble type,  $T$  (G; mainly gleaned from Malkan, Gorjian, & Tam 1998, or RC3 catalog, or Whittle 1992A, Lipovetsky et al. 1988) for the final list of objects for the two Seyfert sub-classes.

where

$$(\Delta m)_{\text{disk}} = 0.324\tau - 0.054\tau^2 + 0.0047\tau^3,$$

where  $\tau = T + 5$ , and  $T$  is the Hubble type (Sandage 1975). Figure 1E shows the distribution of the absolute bulge luminosity,  $M_B^{\text{bulge}}$ , of the host galaxy for the two Seyfert sub-classes. We therefore tried to ensure that our two sub-samples did not differ significantly in the distribution of this parameter.

#### 2.4.5. Hubble type of the host galaxy

The Hubble type mainly depends on the size of the nuclear bulge relative to the flattened disk (Sandage 1975). Malkan, Gorjian, & Tam (1998) have argued that the Seyfert 1 galaxies are of earlier Hubble type than Seyfert 2 galaxies. We therefore have considered the distribution of Hubble type of the host galaxy for our sample of Seyfert 1 and Seyfert 2 galaxies. We use the Hubble type given in the RC3 catalog (de Vaucouleurs et al. 1991) for our sample sources, and when not available, we use values from Whittle (1992A) or Lipovetsky et al. (1988). The Hubble type of one of the objects, Mrk 1218, which was unavailable in de Vaucouleurs et al. (1991), Whittle (1992A), and Lipovetsky et al. (1988), is taken from Malkan, Gorjian, & Tam (1998). The distributions are shown

in Figure 1F and are statistically not significantly different for the two Seyfert sub-classes. We have thus controlled for the Hubble type in our sample. Since, the morphological class given by Malkan, Gorjian, & Tam (1998) are based on *WFPC2*, *Hubble Space Telescope* images, we also in Figure 1G show the distribution of the Hubble type for the two Seyfert sub-samples where the Hubble types are preferentially gleaned from Malkan, Gorjian, & Tam (1998), 6 out of 10 Seyfert 1 and 7 out of 10 Seyfert 2 galaxies, and then from RC3 catalog or Whittle (1992A) or Lipovetsky et al. (1988).

Thus, of the 126 Seyfert galaxies that had VLA data in the literature, 54 met our feasibility criterion. Twenty nine of these 54 had all the required parameters in the literature. From these 29 we could pick 20 Seyferts that met our selection criteria and were matched in the orientation-independent parameters.

#### 2.5. Our Seyfert sample

Our aim was to study the pc-scale radio morphology of Seyfert galaxies so as to test the predictions of the unified scheme hypothesis. By matching Seyfert 1 and Seyfert 2 galaxies in the above parameters, particularly  $[O\ III]\ \lambda 5007$  luminosity (an indicator of intrinsic AGN power) and stellar luminosity of the host galaxy, we ensured that the sam-

TABLE 2  
TABLE SHOWING THE LIST OF SEYFERT 1 AND SEYFERT 2 GALAXIES THAT CONSTITUTE OUR SAMPLE, WITH THE ORIENTATION-INDEPENDENT PARAMETERS THAT WERE USED TO CONSTRAINT IT.

Object	VLA A array compact		Redshift	[O III]	$\frac{F_{\lambda 5007}}{F_{H\beta}}$	[O III]	$M_B^{\text{total}}$	$M_B^{\text{bulge}}$	T	T
	(b/a)	component		line width		luminosity				
(1)	(2)	$S_\nu$ (mJy)	(4)	(km s <sup>-1</sup> )	(6)	(7)	(8)	(9)	(10)	(11)
Seyfert 1s										
MCG 8-11-11	0.71	32.5	0.025	605.0 <sup>3</sup>	3.5 <sup>1</sup>	42.14 <sup>3</sup>	-23.1 <sup>3</sup>	-22.10	1 <sup>9</sup>	0
Mrk 1218	0.58	23.0	0.029	1078.0 <sup>6</sup>	3.8 <sup>3</sup>	41.82 <sup>1</sup>	-21.1 <sup>7</sup>	-20.04	1 <sup>10</sup>	1
NGC 2639	0.60	23.4	0.011	400.0 <sup>2</sup>	0.3 <sup>7</sup>	39.88 <sup>2</sup>	-21.4 <sup>7</sup>	-20.33	1 <sup>11</sup>	3
NGC 4151	0.71	34.0	0.003	425.0 <sup>3</sup>	3.3 <sup>1</sup>	42.19 <sup>3</sup>	-21.2 <sup>3</sup>	-19.99	2 <sup>11</sup>	
Mrk 766	0.87	14.5	0.013	180.0 <sup>3</sup>	3.7 <sup>3</sup>	41.77 <sup>3</sup>	-21.0 <sup>3</sup>	-20.01	1 <sup>11</sup>	3
Mrk 231	0.74	155.0	0.042	> 600.0 <sup>5</sup>	0.4 <sup>1</sup>	40.27 <sup>1</sup>	-22.3 <sup>7</sup>	-19.75	5 <sup>11</sup>	
Ark 564	0.65	8.0	0.024	240.0 <sup>3</sup>	1.0 <sup>3</sup>	41.72 <sup>c</sup>	-21.7 <sup>3</sup>	-20.11	3 <sup>9</sup>	
NGC 7469	0.72	21.0	0.016	360.0 <sup>3</sup>	0.6 <sup>3</sup>	41.84 <sup>3</sup>	-22.0 <sup>3</sup>	-20.99	1 <sup>11</sup>	4
Mrk 926	0.67	9.0	0.047	365.0 <sup>3</sup>	0.6 <sup>1</sup>	42.53 <sup>3</sup>	-22.4 <sup>3</sup>	-21.39	1 <sup>9</sup>	
Mrk 530	0.66	10.0	0.030	490.0 <sup>3</sup>	0.3 <sup>1</sup>	41.26 <sup>3</sup>	-22.7 <sup>3</sup>	-21.20	3 <sup>11</sup>	1
Seyfert 2s										
Mrk 348	1.00	480.0	0.015	365.0 <sup>3</sup>	10.5 <sup>3</sup>	41.69 <sup>3</sup>	-21.1 <sup>3</sup>	-20.27	0 <sup>11</sup>	0
Mrk 1	0.62	26.0	0.016	520.0 <sup>3</sup>	11.1 <sup>3</sup>	41.85 <sup>3</sup>	-20.3 <sup>3</sup>	-19.46	0 <sup>9</sup>	5
NGC 2273	0.76	8.9	0.006	110.0 <sup>3</sup>	10.0 <sup>3</sup>	40.92 <sup>3</sup>	-21.0 <sup>3</sup>	-19.97	1 <sup>11</sup>	3
Mrk 78	0.55	8.0	0.037	1075.0 <sup>3</sup>	13.2 <sup>3</sup>	42.62 <sup>3</sup>	-22.0 <sup>3</sup>	-20.78	1 <sup>9</sup>	
NGC 5135	0.71	15.8	0.014	165.0 <sup>3</sup>	5.1 <sup>3</sup>	41.28 <sup>3</sup>	-22.1 <sup>3</sup>	-20.91	2 <sup>11</sup>	5
Mrk 477	0.78	18.3	0.038	370.0 <sup>3</sup>	8.8 <sup>3</sup>	43.02 <sup>3</sup>	-21.0 <sup>3</sup>	-20.13	0 <sup>12</sup>	
NGC 5929	0.93	13.5	0.009	415.0 <sup>3</sup>	4.0 <sup>3</sup>	40.63 <sup>3</sup>	-21.4 <sup>3</sup>	-20.13	2 <sup>11</sup>	0
NGC 7212	0.50	30.0	0.027	435.0 <sup>3</sup>	10.8 <sup>3</sup>	42.34 <sup>3</sup>	-21.2 <sup>3</sup>	-20.22	1 <sup>9</sup>	
Mrk 533	0.78	27.0	0.029	350.0 <sup>3</sup>	12.9 <sup>3</sup>	42.26 <sup>3</sup>	-22.7 <sup>3</sup>	-20.68	4 <sup>11</sup>	5
NGC 7682	0.89	13.5	0.017	255.0 <sup>3</sup>	> 4.0 <sup>3</sup>	41.46 <sup>3</sup>	-21.1 <sup>3</sup>	-19.88	2 <sup>11</sup>	0

REFERENCES. — (1) Dahari & De Robertis (1988); (2) Keel (1983); (3) Whittle (1992A); (4) see Section 2.4.4; (5) Kim et al. (1998); (6) Goodrich (1989); (7) see Section 2.4.3; (8) see Section 2.4.5; (9) Whittle (1992A); (10) Malkan, Gorjian, & Tam (1998); (11) de Vaucouleurs et al. (1991); (12) Lipovetsky et al. (1988).

NOTE. — Col. (1), source name; col. (2), ratio of minor to major isophotal axes of the host galaxies (all entries are from RC3 catalog (de Vaucouleurs et al. 1991) except for Mrk 926 source, which is from Lipovetsky et al. (1988)); col. (3), core flux densities on arcsec-scale resolution (flux density of the detected compact core component at  $\lambda_{6\text{ cm}}$  on arcsec-scale resolution. NGC 7212: Correlated flux density detected at 13 cm by Roy et al. (1994) using the PTI interferometer. Mrk 533 and NGC 7682: The measurements are at  $\lambda_{3.6\text{ cm}}$  on arcsec-scale resolution); col. (4), cosmological redshift; col. (5), [O III]  $\lambda 5007$  emission line widths; col. (6), line intensity ratios of [O III]  $\lambda 5007$  and H $\beta$ ; col. (7), luminosities of the [O III]  $\lambda 5007$  emission line; col. (8), stellar luminosities of the host galaxies; col. (9), absolute bulge luminosities of the host galaxies; col. (10), Hubble types of the host galaxies (see Section 2.4.5—the morphological class (Hubble type) given in RC3 catalog (de Vaucouleurs et al. 1991) for our sample sources and when not available, we use values from, in order, Whittle (1992A), or Lipovetsky et al. (1988), or Malkan, Gorjian, & Tam (1998)); col. (11), same as col. (10), but the morphological class preferentially gleaned from Malkan, Gorjian, & Tam (1998), which are based on WFPC2, *HST* images, RC3 catalog, or Whittle (1992A), or Lipovetsky et al. (1988).

ples of Seyfert 1 and Seyfert 2 galaxies were intrinsically similar within the framework of unified scheme. Table 2 lists our sample of Seyfert galaxies giving all the orientation-independent parameters that were used to construct it, *viz.*, ratio of minor to major axis of the host galaxy, the radio flux density of the compact component, cosmological redshift, [O III]  $\lambda 5007$  emission line width, the ratio of emission line intensities of fluxes in [O III]  $\lambda 5007$  to H $\beta$ , luminosity of the [O III]  $\lambda 5007$  emission line, stellar luminosity of the host galaxy, bulge absolute luminosity of the host galaxy, and Hubble type for the two Seyfert sub-classes.

The fact that we avoided edge-on host galaxies results in a selection of samples of Seyfert 1 and Seyfert 2 galaxies differing in one intrinsic respect. Thus it follows that our sample has a paucity of Seyfert 1 galaxies with their radio-jets in the plane of the host galaxy and similarly there is a paucity of Seyfert 2 galaxies with their jet-axis perpendicular to the plane of the host galaxy. If the gaseous interstellar medium (ISM) of the host galaxy has an effect on the propagation of the jet through it, then it implies that there is a physical difference in this respect between our Seyfert 1 and Seyfert 2 galaxies. However this is unlikely, since many studies indicate that the orientation of the AGN axis (and therefore the radio-jet)

relative to the host galaxy axis is random (Schmitt et al. 2001; Pringle et al. 1999; Nagar & Wilson 1999), and radio-jets on all angular/linear scales are seen in all orientations.

In Lal, Shastri, & Gabuzda (2004), we presented the radio images that were obtained from our observations (project code GL022, date of observations February 18, 1998) and described the properties at these scales in the light of past observations. The data from these observations along with published radio data for the unobserved (well studied) sources, *viz.* Mrk 348, NGC 4151, Mrk 231 and Mrk 926 at both pc-scale and kpc-scales and NGC 5135 at kpc-scales are used to discuss the impact on the unified scheme hypothesis. Table 3 lists the derived parameters (our and published radio data) for our Seyfert galaxy sample; the sequence of sources is ordered in right ascension.

### 3. INTERPRETATION

**The contradiction with the unification scheme and its resolution:** Roy et al. (1994) observed far-infrared selected, mid-infrared selected and optically selected samples of Seyfert galaxies with a 275 km long, single-baseline, the Parkes-Tidbinbilla Interferometer (PTI, Norris et al. 1988, 1992B) at 1.7 and 2.3 GHz. They reported that compact ra-

TABLE 3  
TABLE GIVING DERIVED PARAMETERS FOR OUR SEYFERT GALAXY SAMPLE (SOURCES ARE ORDERED IN INCREASING RIGHT ASCENSION).

Object	Distance	$S_{\nu}^{\text{total}}$ (arcmin <sup>-2</sup> )	$S_{\nu}^{\text{total}}$ (arcsec <sup>-2</sup> )	$S_{\nu}^{\text{core}}$ (arcsec <sup>-2</sup> )	$S_{\nu}^{\text{total}}$ (mas <sup>-2</sup> )	$L^{\text{total}}$ (1.4 GHz)	$L^{\text{total}}$ (kpc-scale)	$L^{\text{core}}$ (kpc-scale)	$L^{\text{total}}$ (pc-scale)	Size
(1)	(Mpc)	(3)	(4)	(5)	(6)	(7)	(8)	(9)	(10)	(log(size)) (pc)
Mrk 348	59.6	277.3	346.0 <sup>1</sup>	310.3 <sup>1</sup>	163.0 <sup>2</sup>	$1.2 \times 10^{30}$	$1.5 \times 10^{30}$	$1.3 \times 10^{30}$	$7.0 \times 10^{29}$	1.76 <sup>10</sup>
Mrk 1	63.5	70.8	27.8	24.1	4.4	$3.5 \times 10^{29}$	$1.4 \times 10^{29}$	$1.2 \times 10^{29}$	$2.1 \times 10^{28}$	< 2.30 <sup>11</sup>
MCG 8-11-11	98.8	228.3	78.0	23.6	4.9	$2.7 \times 10^{30}$	$9.1 \times 10^{29}$	$2.8 \times 10^{29}$	$5.9 \times 10^{28}$	3.22 <sup>11</sup>
NGC 2273	23.9	59.7	22.0	12.1	6.3	$4.1 \times 10^{28}$	$1.4 \times 10^{28}$	$8.4 \times 10^{27}$	$4.4 \times 10^{27}$	2.42 <sup>11</sup>
Mrk 78	145.4	35.0	13.1	8.9	8.5	$9.2 \times 10^{29}$	$2.8 \times 10^{29}$	$2.3 \times 10^{29}$	$2.1 \times 10^{29}$	3.43 <sup>11</sup>
Mrk 1218	114.4	63.6	27.7	18.7	12.3	$1.0 \times 10^{30}$	$3.9 \times 10^{29}$	$3.0 \times 10^{29}$	$1.2 \times 10^{29}$	2.85 <sup>11</sup>
NGC 2639	43.8	105.5	85.8	63.5	39.5	$2.5 \times 10^{29}$	$1.9 \times 10^{29}$	$1.5 \times 10^{29}$	$9.2 \times 10^{28}$	< 2.14 <sup>11</sup>
NGC 4151	12.0	345.8	120.0 <sup>3</sup>	43.0 <sup>3</sup>	10.0 <sup>4</sup>	$6.0 \times 10^{28}$	$2.0 \times 10^{28}$	$7.4 \times 10^{27}$	$3.5 \times 10^{27}$	2.57 <sup>14</sup>
Mrk 766	51.7	37.6	17.9	13.8	3.6	$1.2 \times 10^{29}$	$4.9 \times 10^{28}$	$4.5 \times 10^{28}$	$1.2 \times 10^{28}$	< 2.21 <sup>11</sup>
Mrk 231	164.6	282.9	282.0 <sup>5</sup>	270.0 <sup>5</sup>	173.0 <sup>5</sup>	$9.6 \times 10^{30}$	$5.9 \times 10^{30}$	$5.5 \times 10^{30}$	$2.3 \times 10^{30}$	< 2.37 <sup>14</sup>
NGC 5135	55.6	190.0	58.8 <sup>6</sup>	16.2 <sup>6</sup>		$7.2 \times 10^{29}$	$2.2 \times 10^{29}$	$6.1 \times 10^{28}$		3.28 <sup>12</sup>
Mrk 477	149.2	60.7	27.3	23.0	8.1	$1.7 \times 10^{30}$	$6.8 \times 10^{29}$	$6.6 \times 10^{29}$	$2.3 \times 10^{29}$	< 2.86 <sup>13</sup>
NGC 5929	35.8	105.5	34.4	1.3 <sup>7</sup>	6.2	$1.6 \times 10^{29}$	$4.9 \times 10^{28}$	$2.0 \times 10^{27}$	$9.8 \times 10^{27}$	2.78 <sup>11</sup>
NGC 7212	106.6	108.9	31.0	19.6	7.0	$1.5 \times 10^{30}$	$4.8 \times 10^{29}$	$2.7 \times 10^{29}$	$9.2 \times 10^{28}$	3.20 <sup>11</sup>
Ark 564	94.9	27.7	11.4	8.6	3.2	$3.1 \times 10^{29}$	$1.3 \times 10^{29}$	$9.5 \times 10^{28}$	$3.6 \times 10^{28}$	< 2.59 <sup>11</sup>
NGC 7469	63.5	167.7	47.9	22.0	6.1	$8.3 \times 10^{29}$	$2.1 \times 10^{29}$	$1.1 \times 10^{29}$	$3.0 \times 10^{28}$	2.93 <sup>11</sup>
Mrk 926	183.8	33.0	9.0 <sup>8</sup>	7.7 <sup>8</sup>	5.0 <sup>9</sup>	$1.4 \times 10^{30}$	$3.8 \times 10^{29}$	$3.3 \times 10^{29}$	$2.1 \times 10^{29}$	3.07 <sup>15</sup>
Mrk 530	118.3	23.5	10.2	8.0	8.6	$4.6 \times 10^{29}$	$1.6 \times 10^{29}$	$1.4 \times 10^{29}$	$1.5 \times 10^{29}$	< 2.67 <sup>11</sup>
Mrk 533	114.4	206.4	58.8	38.2	16.9	$3.3 \times 10^{30}$	$9.7 \times 10^{29}$	$6.2 \times 10^{29}$	$2.7 \times 10^{29}$	3.02 <sup>11</sup>
NGC 7682	67.4	58.6	22.6	22.0	11.5	$3.3 \times 10^{29}$	$1.2 \times 10^{29}$	$1.2 \times 10^{29}$	$5.0 \times 10^{28}$	< 2.49 <sup>11</sup>

REFERENCES. — (1) Nov 1996, VLA 8.4 GHz measurement (Thean et al. 2001); (2) Apr 1995, VLBA 8.4 GHz measurement (Barvainis & Lonsdale 1998); (3) Mar 1980, VLA 5.0 GHz measurement (Johnston et al. 1982); (4) May/June 1996, VLBA 5.0 GHz measurement (Ulvestad et al. 1998); (5) Dec 1996, VLA 5.0 GHz measurement (Ulvestad et al. 1999A); (6) Feb 1985, VLA 5.0 GHz measurement (Ulvestad & Wilson 1989); (7) Mar 1989, MERLIN measurements and  $\alpha_{18\text{cm}}^2 = 0.32$ ; (Su et al. 1996); (8) May 1982, VLA 5.0 GHz measurement (Ulvestad & Wilson 1984A,B); (9) Jul 1997, VLBA 8.4 GHz measurement (Mundell et al. 2000); (10) (Unger et al. 1984); (11) Our (Lal, Shastri, & Gabuzda 2004) measurements; (12) (Ulvestad & Wilson 1989); (13) (Pedlar et al. 1993); (14) (Kukula et al. 1995); (15) (Ulvestad & Wilson 1984A).

NOTE. — Col. (1), source name; col. (2), distance to the source assuming a cosmology with  $H_0 = 75 \text{ km s}^{-1} \text{ Mpc}^{-1}$  and  $q_0 = 0$ ; col. (3), total flux density on arcmin-scale at 1.4 GHz (NVSS: Condon et al. 1998); col. (4), total flux density on arcsec-scale at 5 GHz; col. (5), core flux density on arcsec-scale at 5 GHz; col. (6), core flux density on mas-scale at 5 GHz; col. (7), radio power on arcmin-scale at 1.4 GHz (NVSS: Condon et al. 1998); col. (8), total radio power on arcsec-scale at 5 GHz; col. (9), core radio power on arcsec-scale at 5 GHz; col. (10), core radio power on mas-scale at 5 GHz; col. (11), logarithm of the projected linear size on mas-scale at 5 GHz.

radio structures are much more common in Seyfert 2 than in Seyfert 1 galaxies in the far-infrared selected samples, as well as in the combined mid-infrared and optically selected sample. They deduced this result based on significantly different detection rate of compact, high brightness temperature radio structure. Their surprising result that far-infrared selected Seyfert 1 galaxies were detected less frequently than were Seyfert 2 galaxies is inconsistent with the standard unification scheme. The unified scheme would predict an equal fraction of detections for Seyfert 1 and Seyfert 2 galaxies. It is also the opposite sense of what is expected from alternative models in which Seyfert 1 galaxies are expected to have more energetic cores than Seyfert 2 galaxies. Also, even if the jets were relativistically beamed, we would expect Seyfert 1 galaxies to show systematically more prominent compact radio emission than Seyfert 2 galaxies, since they are the face-on objects, and it is their jets that would be pointed towards us and therefore Doppler beamed.

However, Roy et al. (1994) invoked a model which attempts to reconcile their result with the unification scheme. They considered the radio optical depth due to the free-free absorption of the NLR clouds which surround the radio emitting regions of the core and NLR, which is in line with the model first proposed by Norris et al. (1992A). There could be two distinct mechanisms; (i) obscuration by the NLR and (ii) obscuration by individual NLR clouds that may contribute to the resulting radio appearance. These two mechanisms invoke

free-free absorption by the NLR clouds, which is highly dependent on the geometry of the NLR, the opening angle of the cone (anisotropic escape of photons is in the form of a cone), and the filling factor. In contrast to Roy et al.'s (1994) result, all 19 of our 20 sample sources for which VLBI observations are available have compact features. We do not find any systematically different detection rate of compact structures. We thus find that Seyfert 1 and Seyfert 2 galaxies have an equal tendency to show compact radio structures, in contrast to the results of Roy et al. (1994). Although we chose sources with core flux density  $> 8 \text{ mJy}$  for the feasibility requirements, our result is thus consistent with the prediction of the simple unified scheme for such a Seyfert sample. Figure 2A shows the distribution of brightness temperatures,  $T_b$ , of the brightest component detected at 5 GHz on mas-scales and Figure 2B shows the distribution of the ratio of flux density detected on mas-scales, to that detected on arcsec-scales. Mann-Whitney U test shows that the two distributions (Figures 2A and 2B) are same at a significance level of 0.10. These distributions show that the brightness temperatures of the brightest component detected on mas-scales and the fraction of total flux density detected on mas-scales are not different for the two groups of Seyfert galaxies. Note that our pc-scale and kpc-scale data are simultaneous, and hence, the statistically similar ratio of flux density detected on mas-scales to that detected on arcsec-scales for the two Seyfert sub-classes is not affected by possible radio variability in the compact ra-

dio flux densities in 15 out of 20 cases. This demonstrates that the fact that our detection rate is higher than Roy et al.'s (1994) is not just due to the higher sensitivity of the interferometer we used.

### 3.1. Pc-scale radio luminosities

We derive the observed radio luminosity from the observed flux density  $S_\nu$  via

$$L_\nu = 4\pi S_\nu (d)^2 (1+z),$$

where  $d = \frac{cz(1+(z/2))}{H_0(1+z)}$ , and we use

$$H_0 = 75 \text{ kms}^{-1} \text{ Mpc}^{-1} \text{ and } q_0 = 0.$$

The values are given in Table 3 and Figure 2C shows the distribution of the radio luminosity detected on pc-scales for the two Seyfert sub-classes. The distribution shows that the pc-scale radio luminosities of the Seyfert 1 and the Seyfert 2 galaxies are similar. The Mann-Whitney U test shows that the distributions are statistically indistinguishable at a significance level of 0.05. Thus the distribution of pc-scale radio luminosities of Seyfert 1 and Seyfert 2 galaxies are consistent with the unified scheme hypothesis.

### 3.2. Kpc-scale radio luminosities

Figure 2D shows the distribution of the radio luminosity detected on kpc-scales for the two Seyfert sub-classes. The Mann-Whitney U test shows that there is no statistically significant difference in the distribution at a significance level of 0.10. The Mann-Whitney U test also shows that there is no statistically significant difference in the distribution of core (the component of the source which is the closest to the optical nucleus within errorbars) radio luminosity (Figure 2E) on arcsec-scales for the two Seyfert sub-classes at a significance level of 0.10. Our results are thus consistent with the predictions of the unification scheme hypothesis and are also consistent with the results of Nagar et al. (1999) but are inconsistent with Morganti et al. (1999), who found that Seyfert 2 galaxies tend to be more luminous than Seyfert 1 galaxies at marginal significance. The NRAO VLA Sky Survey (NVSS, Condon et al. 1998) radio observations are made at 1.4 GHz using VLA *D* configuration. All our sample objects have measurements made using this instrument. Figure 2F shows that the two histograms of Seyfert 1 and Seyfert 2 galaxies are statistically indistinguishable for total 1.4 GHz radio luminosity on arcmin-scales at a significance level of 0.05 using Mann-Whitney U test, which is again consistent with the unified scheme hypothesis.

### 3.3. Projected linear sizes

The linear sizes of Seyfert galaxies can be used to test the unification scheme because Seyfert 1 galaxies oriented at small angles to the line of sight should have systematically smaller linear sizes than Seyfert 2 galaxies in the plane of the sky. For their distance limited sample of Seyfert galaxies, Morganti et al. (1999) found Seyfert 1 to be of systematically smaller sizes than Seyfert 2 galaxies. This is consistent with the prediction of the unified scheme. We determine the projected linear size of the source using

$$\text{Linear size} = (\text{angular size}) \times \left( \frac{(cz)(1+(z/2))}{H_0} \right);$$

for  $q_0 = 0$ . Here,  $c$  is the velocity of light,  $H_0$  is the Hubble parameter and  $z$  is the redshift of the object. We assume that the largest angular size of the source is the largest extent of the contour that is 5% of the peak surface brightness level, which is well above the noise level and use it to determine the linear radio size of the source. For Mrk 348 (Unger et al. 1984), NGC 4151, Mrk 231 (Kukula et al. 1995), NGC 5135 (Ulvestad & Wilson 1989), and Mrk 926 (Ulvestad & Wilson 1984A), we measure their corresponding largest angular sizes directly from the published maps. Table 3 gives the projected linear size of the source along with the reference, and Figure 2G shows the distribution of projected linear size for our sample of Seyfert 1 and Seyfert 2 galaxies. The Mann-Whitney U test shows that the distributions are not significantly different at a significance level of 0.10. It thus appears that the intrinsic variation in the projected linear sizes is rather large and may swamp any systematic difference between Seyfert 1 and Seyfert 2 galaxies due to projection. Further, if the ISM of the host galaxy affects the propagation of a Seyfert galaxy radio-jet, the fact that our sample has a paucity of Seyfert 2 galaxies with jet direction perpendicular to the plane of the host galaxy and Seyfert 1 galaxies with their jets propagating in the plane of the host galaxy disk, may also contribute to reduce the systematic differences in projected linear sizes between Seyfert 1 and Seyfert 2 galaxies.

We also show the scatter plot of the radio luminosity on kpc-scales *versus* the projected linear size in Figure 3. Including the upper-limits to the linear size, the correlation is significant (Spearman's rank correlation coefficient = 0.91) for the Seyfert 1 and Seyfert 2 galaxies taken together. Thus, even though we restricted the range of the intrinsic AGN power for our sample, we still find a significant correlation of these two parameters, earlier noted by Ulvestad & Wilson (1989) and Morganti et al. (1999). Mrk 348 is one of our outliers, and is noted by Morganti et al. (1999); a projected linear size of 5 kpc (Baum et al. 1993) for this source puts it closer to the correlation.

### 3.4. Source spectral indices

The unified scheme predicts that Seyfert 1 and 2 galaxies arise from the same parent population of AGN, and the derived orientation-independent parameters should not show significantly different distributions. Morganti et al. (1999) did not find significantly different distribution of spectral index for Seyfert 1 and Seyfert 2 galaxies. We use our observations along with measurements at 2.0 cm, 3.6 cm, 6.0 cm and 20.0 cm, preferably VLA *A* or *B* configuration observations (when not available we use coarser resolution measurements) to determine the spectral indices,  $\alpha_{20 \text{ cm}}^6 \text{ cm}$ ,  $\alpha_{6 \text{ cm}}^{3.6 \text{ cm}}$ , and  $\alpha_{3.6 \text{ cm}}^2 \text{ cm}$ , of the total flux density emitted (core plus the extended radio emission) of the source. Table 4 gives the measured flux densities and the spectral indices for our Seyfert sample. Mrk 348 and Mrk 231 show radio variability (Lal 2002). Mundell et al. (2009) using VLA at 8.4 GHz have shown that five sources from their sample of 12 optically selected, early-type Seyfert galaxies show radio variability. In this regard, we have attempted to use data that were obtained as near in time as possible to ours, and with angular resolution as close as possible to ours when calculating spectral indices using our own data or data from the literature. Mrk 231 between 1.4 and 5.0 GHz, Mrk 348 between 1.4 and 8.4 GHz, MCG 8-11-11 between 5.0 and 15 GHz, and NGC 5929 between 1.4 and 15 GHz show flat spectrum ( $\alpha \leq 0.4$ ) radio cores. Figure 2H shows the distribution of the source spectral index,  $\alpha_{20 \text{ cm}}^6 \text{ cm}$  be-



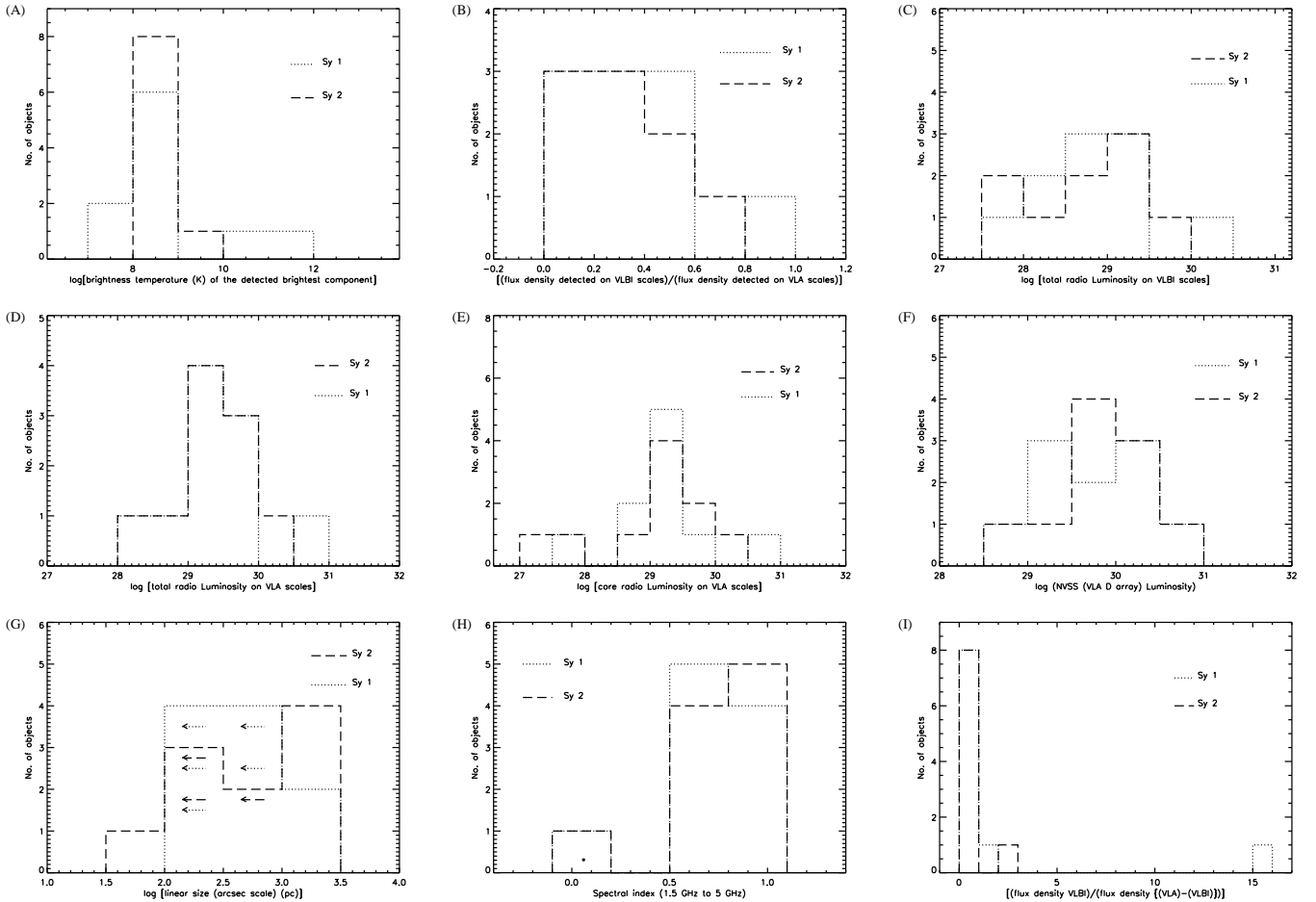


FIG. 2.— Histograms showing distributions of brightness temperature,  $T_b$ , of the brightest component detected on mas-scales (A), ratio of the flux density detected on mas-scales to the flux density detected on arcsec-scales (B), total radio luminosity ( $\text{ergs s}^{-1}\text{Hz}^{-1}$ ) on mas-scales (C), total radio luminosity ( $\text{ergs s}^{-1}\text{Hz}^{-1}$ ) on arcsec-scales (D), core radio luminosity ( $\text{ergs s}^{-1}\text{Hz}^{-1}$ ) on arcsec-scales (E), total radio luminosity ( $\text{ergs s}^{-1}\text{Hz}^{-1}$ ) on arcmin-scales at 1.4 GHz (F), projected radio linear size (pc) on arcsec-scales; arrows denote objects that are unresolved (G), spectral indices between 1.5 and 5 GHz; the spectral index between 1.5 and 8.4 GHz is used for Mrk 348, denoted by asterisk (H), and the fraction of the total radio flux density detected on mas-scales as against the extended radio emission,  $R$  (I).

tween 1.5 GHz (or 1.4 GHz) and 5 GHz (except for Mrk 348, where it is plotted between 5.0 GHz and 8.4 GHz). The Mann-Whitney U test shows that the distributions are statistically indistinguishable at a significance level of 0.02. Our result at the stated significance level is consistent with the prediction of the unified scheme, which does not have any preference for either kind of Seyfert galaxies to show flat/steep source spectrum.

### 3.5. Relativistic beaming in Seyfert galaxies?

In radio loud objects when the emitting plasma has bulk relativistic motion relative to a fixed observer, its emission is Doppler enhanced or beamed in the forward direction (in the fixed frame), a direct consequence of the transformation of angles in special relativity. An observer located in or near the path of this plasma sees much more intense emission than if the same plasma were at rest. Strong relativistic beaming is thought to explain the superluminal motion and high luminosities that characterize blazars (Blandford & Rees 1978). If present in blazars, it may also be present in other AGNs where the radio-jet is pointed close to the line of sight of the observer. Blandford & Königl (1979) formulated the theory of bulk relativistic motion for a two-component “jet version” of

the original model, and explored some of the consequences. In this model, the radio emission originates within a collimated supersonic jet that supplies the extended radio lobes with mass, momentum and energy. The required *in situ* acceleration of the emitting particles is achieved by means of mildly relativistic shocks propagating into the plasma and confined to a jet. The “fixed” component observed in the VLBI observations is identified in this model with the base of the jet. One of the direct consequences of this bulk relativistic motion is that when the motion is in directions close to the line of sight, the observed radio flux density is apparently enhanced due to Doppler effects. The observed flux density  $S_{\text{obs}}$  of the jet at a frequency  $\nu$  is related to the emitted flux density  $S_{\text{em}}$  that would be observed in the comoving frame at the same emitted frequency  $\nu$  as

$$S_{\text{obs}} = S_{\text{em}} D^3.$$

$D$ , the Doppler factor, is the ratio of observed to emitted frequency and is given by

$$D = \gamma^{-1} (1 - \frac{v}{c} \cos \theta)^{-1},$$

TABLE 4  
SOURCE TOTAL FLUX DENSITIES AND SPECTRAL INDICES; WE DEFINE THE SPECTRAL INDEX  $\alpha$  IN THE SENSE THAT  $S_\nu \propto \nu^{-\alpha}$ , WHERE  $S_\nu$  AND  $\nu$  ARE FLUX DENSITY AND FREQUENCY, RESPECTIVELY.

Object	Total flux density				Spectral index (total)				References
	$S_{1.5 \text{ GHz}}$	$S_{5.0 \text{ GHz}}$	$S_{8.4 \text{ GHz}}$	$S_{15 \text{ GHz}}$	$\alpha_{20 \text{ cm}}^{3.6 \text{ cm}}$	$\alpha_{20 \text{ cm}}^{6 \text{ cm}}$	$\alpha_{6 \text{ cm}}^{3.6 \text{ cm}}$	$\alpha_{3.6 \text{ cm}}^{2 \text{ cm}}$	
Mrk 348	302.2		238.0		0.14				1.5 GHz–1, 8.4 GHz–1
Mrk 1	68.0	27.65	15.4		0.86	0.75	1.13		1.5 GHz–2, 5.0 GHz–3, 8.4 GHz–4
MCG 8-11-11	180.0	75.76	38.4	20.0	0.90	0.72	1.31	1.13	1.5 GHz–5, 5.0 GHz–3, 8.4 GHz–4, 15 GHz–6
NGC 2273	52.0	19.92	10.2		0.95	0.80	1.29		1.5 GHz–1, 5.0 GHz–3, 8.4 GHz–1
Mrk 78	31.0	10.46				0.90			1.5 GHz–7, 5.0 GHz–3
Mrk 1218	65.0	24.04				0.83			1.5 GHz–6, 5.0 GHz–3
NGC 2639	104.0	54.50				0.54			1.5 GHz–8, 5.0 GHz–8
NGC 4151	330.0	120.00	72.32	23.9	0.88	0.84	0.98	1.91	1.5 GHz–9, 5.0 GHz–9, 8.4 GHz–10, 15 GHz–11
Mrk 766	39.3	15.16	8.68		0.88	0.79	1.09		1.5 GHz–1, 5.0 GHz–3, 8.4 GHz–1
Mrk 231	280.0	355.00		< 284.0		–0.20			All measurements are from 12
NGC 5135	163.2	58.80				0.85			1.5 GHz–8, 5.0 GHz–8
Mrk 477	60.7	24.39				0.76			1.5 GHz–NVSS, 5.0 GHz–3
NGC 5929	64.7	31.74	16.75	9.0	0.78	0.59	1.23	1.07	All measurements are from 13
NGC 7212	108.8	33.94	> 9.0			0.97			1.5 GHz–NVSS, 5.0 GHz–3, 8.4 GHz–14
Ark 564	27.7	11.30	7.0			0.74	0.92		1.5 GHz–NVSS, 5.0 GHz–3, 8.4 GHz–4
NGC 7469	134.0	43.56	15.97	8.0	1.23	0.93	1.93	1.19	1.5 GHz–5, 5.0 GHz–3, 8.4 GHz–10, 15 GHz–15
Mrk 926	33.0	9.00				1.07			1.5 GHz–NVSS, 5.0 GHz–16
Mrk 530	23.5	9.17	3.26			0.78	2.00		1.5 GHz–NVSS, 5.0 GHz–3, 8.4 GHz–10
Mrk 533	160.0	60.37	39.77		0.81	0.81	0.80		1.5 GHz–5, 5.0 GHz–3, 8.4 GHz–10
NGC 7682	61.6	22.21	13.46		0.88	0.84	0.97		1.5 GHz–17, 5.0–3, 8.4 GHz–10

REFERENCES. — (1) Nagar et al. (1999); (2) de Bruyn & Wilson (1976); (3) Lal, Shastri & Gabuzda (2004); (4) Schmitt et al. (2001); (5) Unger et al. (1986); (6) Ulvestad & Wilson (1986); (7) Ulvestad & Wilson (1984A); (8) Ulvestad & Wilson (1989); (9) Johnston et al. (1982); (10) Kukula et al. (1995); (11) Wilson & Ulvestad (1982); (12) Ulvestad et al. (1999A); (13) Su et al. (1996); (14) Falcke, Wilson, & Simpson (1998); (15) Wilson et al. (1991); (16) Ulvestad & Wilson (1984A); (17) Edelson (1987).

where  $\theta$  is the angle of inclination of the direction of bulk relativistic motion to the line of sight,  $v$  is velocity of the flow, and  $\gamma$  is the Lorentz factor. In this model, wherein the radio core component is constituted of relativistically moving sub-components, the observed flux density would be enhanced by Doppler effects for directions close to the line of sight.

Seyfert galaxies show radio emitting jet-like structures on small scales which appear to be the low-power analogues of jets seen in radio powerful AGNs (Nagar et al. 1999, and references therein). If this AGN-linked radio emission originates from plasma with sub-relativistic bulk motion, the unified scheme would predict that Seyfert 1 and Seyfert 2 galaxies should have similar radio morphologies on all scales and it would be independent of orientation of the Seyfert galaxy. But, if this radio emitting plasma has mildly relativistic bulk speeds (Bicknell et al. 1998; Ulvestad et al. 1999B), the unified scheme would predict that Seyfert 1 galaxies, in which the radio axis is oriented close to the observers line of sight, should show mild Doppler beaming of the radio cores, whereas Seyfert 2 galaxies should not exhibit such behavior. So far, all the relativistically boosted jets with superluminal motion have only been detected in radio-loud objects, except for the Seyfert 1 galaxy, III Zw 2 (Brunthaler et al. 2000). III Zw 2 is a Seyfert 1 galaxy that conforms to our definition of Seyfert galaxies and is the first detection of superluminal motion in a Seyfert nucleus in a spiral galaxy. Observations of the two Seyfert galaxies, Mrk 348 and Mrk 231 by Ulvestad et al. (1999B), showed sub-relativistic expansion in them.

In radio-loud AGN, the core flux density is Doppler enhanced due to relativistic beaming, while the extended flux density (the flux density of the lobes in radio-loud objects) is not enhanced. Therefore, the ratio of the core and extended flux densities becomes a beaming indicator (Kapahi & Saikia 1982). We define an analogous parameter  $R$  for Seyfert galaxies as

$$R = \frac{S_{\nu \text{ compact}}}{S_{\nu \text{ ext}}},$$

where  $S_{\nu \text{ compact}}$  is the flux density that we measure on pc-scales and  $S_{\nu \text{ ext}}$  is defined as the difference of the total flux density detected on kpc-scale and the flux density detected on pc-scales. If the detected pc-scale emission is coming primarily from ejected plasma close to the nucleus, then by comparing the pc-scale radio emission with the kpc-scale extended emission for the two classes of Seyfert galaxies, one could test the relativistic beaming hypothesis. Due to the availability of simultaneous arcsec-scale data (VLA) for our sample objects, we are able to test for the presence of beaming without worrying about possible radio variability (Mundell et al. 2009) in the compact radio flux densities in 15 out of 20 cases. For the rest of the sample objects (which are not observed by us) we use measurements on pc-scales and kpc-scales which are made at epochs as closely spaced in time as possible (see Table 3). Figure 2I shows the distribution of the ratio of the core and extended flux densities,  $R$  for the two Seyfert subclasses. Mann-Whitney U test shows that the distributions are not significantly different at a level of 0.10. In other words, the compact structures detected on pc-scales are not boosted in Seyfert galaxies.

### 3.6. Seyfert nuclei: Starburst or accretion-powered central engine ?

A key question is, whether a compact starburst alone power Seyfert galaxies, thus not requiring the presence of a super-massive black hole in their nuclei. Powerful circumnuclear starbursts have been unambiguously identified in 40 per cent of nearby Seyfert 2 galaxies (Cid Fernandes et al. 2001, 2004; González-Delgado et al. 1998, 2001; Heckman et al. 2001). These starbursts were originally detected by means of either ultraviolet or optical spectroscopy of the central few 100 pc. Several spectroscopic works have detected features of young and intermediate age stellar population (Heckman et al. 1997; González-Delgado et al. 1998, 2001; Storchi-Bergmann et al. 2000), suggesting that these populations are significant, if not

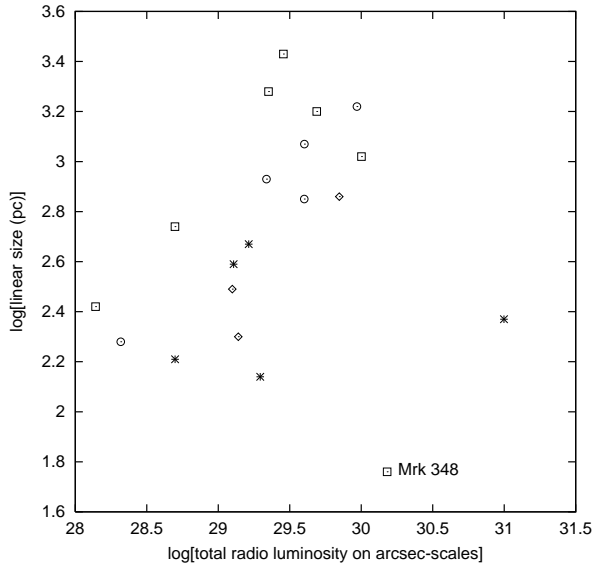


FIG. 3.— Scatter plot of projected linear size (pc) versus radio luminosity on kpc-scales ( $\text{ergs s}^{-1}\text{Hz}^{-1}$ ); symbols  $\circ$ ,  $\square$ ,  $*$ , and  $\diamond$  denotes resolved Seyfert 1, resolved Seyfert 2, unresolved Seyfert 1, and unresolved Seyfert 2 galaxies respectively.

dominant, in the nuclear region of many Seyfert 2 galaxies. Therefore, on a local scale, evidence is mounting that star formation and nuclear activity are linked. Two possible evolutionary progressions can be predicted: H II/Starburst galaxies  $\rightarrow$  Seyfert 2 (Storchi-Bergmann et al. 2001; Kauffmann et al. 2003A,B), or a fuller scenario of H II/Starburst galaxies  $\rightarrow$  Seyfert 2  $\rightarrow$  Seyfert 1 (Hunt & Malkan 1999; Levenson et al. 2001; Krongold et al. 2002). These predict that galaxy interactions, leading to the concentration of a large gas mass in the circumnuclear region of a galaxy, trigger starburst emission. Then mergers and bar-induced inflows can bring fuel to a central black hole, stimulating AGN activity. While emission from the hot stars in the torus might account for the featureless continua in Seyfert 2 galaxies (Cid Fernandes & Terlevich 1995; González-Delgado et al. 1998), starbursts cannot produce the necessary collimation to form radio jets. The existence of radio jets is, therefore, often used as an indication of the presence of a black hole and the accretion disk. Although some Seyfert galaxies are now known to possess strikingly collimated jets (Nagar et al. 1999; Kukula et al. 1995, etc.), the resolution of the radio images is often insufficient to demonstrate the high degree of collimation seen in radio galaxies and radio-loud quasars. For example, although Arp 220 shows a “double-structure” on kpc-scales, pc-scale observations have revealed 13 faint sources in one of the components of the double, interpreted as radio supernovae (Smith, Lonsdale, & Lonsdale 1998). Smith, Lonsdale, & Lonsdale (1998) show that these radio supernovae are of the same class as radio supernova 1986J observed in the disk of NGC 891 (Rupen et al. 1987): Type II radio supernovae with luminosities of order  $10^{28}$   $\text{ergs s}^{-1}\text{Hz}^{-1}$  and exponential decay time of 3 yr. The number of radio supernovae observed in Arp 220 would require a massive star formation rate of  $70 M_{\odot} \text{ yr}^{-1}$  (Parra et al. 2007).

A question that can be addressed with the help of the pc-scale and kpc-scale data for our Seyfert sample (Lal, Shastri, & Gabuzda 2004) is whether the cores

of Seyfert galaxies are primarily made up of radio supernovae. To examine whether compact starbursts alone can power Seyfert galaxies, we consider the following arguments. Cid Fernandes & Terlevich (1995) and González-Delgado et al. (1998) suggest that although emission from hot stars in the torus might account for the featureless continua in Seyfert 2 galaxies, starbursts cannot produce the necessary collimation to form radio jets. We note that elongated radio structures could be attributed to star formation along the galactic plane of a Seyfert host galaxy if it is edge-on (e.g. M 82 a starburst galaxy, Muxlow et al. (1994)). In our sample, however this cannot explain any of the elongated structures, since the sample was selected so as to avoid edge-on host galaxies (ratio of minor to major axis of the host galaxy is greater than 0.5 for all our Seyfert sources). Ulvestad et al. (1999B), on pc-scales, confirmed that Mrk 231 and also Mrk 348 are jet-producing central engine systems. Thus, clearly all objects with elongated or “linear” radio structures, viz., Mrk 348, MCG-8-11-11, NGC 2273, Mrk 78, Mrk 1218, NGC 4151, NGC 5135, NGC 5929, NGC 7212, Mrk 926, and Mrk 533 cannot be powered by a starburst alone. We now try to examine whether radio supernovae or supernova remnants in star forming regions can plausibly be retained as the explanation for those objects in the sample that do not show linear structure, viz. Mrk 1 and NGC 7682 which are essentially compact sources, and NGC 2639, Mrk 477, NGC 7469 and Mrk 530 which are dominated by a compact source but have low surface brightness extensions. Note that Smith, Lonsdale, & Lonsdale (1998) have argued that Mrk 231 cannot be powered by starburst alone.

Although an individual supernova can have brightness temperature higher than the brightness temperature of a radio-quiet quasar (Rupen et al. 1987), the most luminous known radio supernova, 1986J (Rupen et al. 1987), had a peak luminosity of  $\sim 10^{28}$   $\text{ergs s}^{-1}\text{Hz}^{-1}$  at 5 GHz. Given that we have obtained pc-scale flux densities for all the Seyfert galaxies, we find that 0.2 to 240 (median value of around 10) of such supernovae would be needed to power them at 5 GHz (Table 5). Since the typical lifetime of such a supernova event is  $\sim 1$  year, to sustain the observed radio luminosities that we find, a supernova rate of  $\nu_{\text{SN}} \sim 0.2$  to  $240 \text{ yr}^{-1}$  is required. Such rates are in line with those required to power the luminous radio-quiet quasars in the starburst scenario (Parra et al. 2007; Terlevich 1990A,B). However, since our observed luminosities are on pc-scales, and we find evidence for one or several dominant compact components in all our 19 observed Seyfert galaxies, these supernovae must be localized within a few cubic parsec, corresponding to a density  $10^7$  times higher than that observed in M 82 (Muxlow et al. 1994), and higher than in the starburst model of Terlevich & Boyle (1993) by a similar factor. Although the radio emission from starburst region consists of synchrotron radiation from SNRs plus thermal free-free emission from H II regions, the brightness temperature of such a region cannot exceed  $10^5$  K at  $\nu > 1$  GHz (Condon 1992). Using the component size along with its flux density on mas-scales, we find that the brightness temperature,  $T_b$  (Table 5), is in the range of  $\sim 0.4\text{--}7000 \times 10^8$  K for our Seyfert sample. We therefore conclude on the basis of the high brightness temperatures ( $> 10^8$ ), small sizes ( $< 1$  pc), and high supernova rates to explain the detected compact components, that starbursts alone cannot explain the observed radio luminosities in Seyfert galaxies. We can also rule out individual or a collection of extremely bright radio

TABLE 5  
TABLE SHOWING THE BRIGHTNESS  
TEMPERATURE ( $T_b$ ) OF COMPACT BRIGHT  
COMPONENT AND THE SUPERNOVA RATES ( $\nu_{SN}$ )  
NECESSARY TO REPRODUCE RADIO EMISSION  
FOR OUR SAMPLE SOURCES.

Object	$T_b$ (K)	$\nu_{SN}$ ( $yr^{-1}$ )
Mrk 348 <sup>1,2</sup>	$4.4 \times 10^9$	72
Mrk 1	$2.2 \times 10^8$	2
MGC 8-11-11	$4.4 \times 10^8$	6
NGC 2273	$2.6 \times 10^8$	0.4
Mrk 78	$6.1 \times 10^8$	21
Mrk 1218	$2.8 \times 10^8$	17
NGC 2639	$7.0 \times 10^{11}$	9
NGC 4151 <sup>3</sup>	$3.7 \times 10^7$	0.2
Mrk 766	$2.8 \times 10^8$	1
Mrk 231 <sup>4</sup>	$2.6 \times 10^{10}$	240
NGC 5135	$2.3 \times 10^8$	24
Mrk 477	$2.3 \times 10^8$	24
NGC 5929	$5.3 \times 10^8$	1
NGC 7212	$3.0 \times 10^8$	10
Ark 564	$2.5 \times 10^8$	4
NGC 7469	$3.8 \times 10^8$	3
Mrk 926 <sup>2</sup>	$9.7 \times 10^7$	22
Mrk 530	$5.9 \times 10^8$	15
Mrk 533	$4.3 \times 10^8$	28
NGC 7682	$2.9 \times 10^8$	5

REFERENCES. — (1) Barvainis & Lonsdale (1998);  
(2) Mundell et al. (2000); (3) Ulvestad et al. (1998); (4)  
Ulvestad et al. (1999A).

supernovae as an explanation for the compact emission from the Seyfert galaxies.

### 3.7. CfA Seyfert galaxy sample: Kpc-scale radio morphology

The CfA Seyfert sample (Huchra & Burg 1992) is drawn from 2399 galaxies in the CfA Redshift survey (Davis et al. 1983; Huchra et al. 1983) and consists of 48 objects (24 Seyfert 1.0 & Seyfert 1.5, 4 Seyfert 1.8, 4 Seyfert 1.9, and 15 Seyfert 2.0) chosen solely on the basis of strong emission lines in their spectra. Kukula et al. (1995) made observations of the optically selected complete spectroscopic sample at 8.4 GHz with the VLA in *A* and *C* configuration in 1991 June and 1992 April respectively, and the observational results of the sample along with individual source morphology, radio maps, flux densities, etc. have been presented in their paper. Note that the unresolved optical nucleus of a Seyfert grows fainter with the square of distance, whilst the surface brightness of its host galaxy remains constant over a constant aperture. In other words, in this sample, the ratio of the two components (the host galaxy to the active nucleus surface brightness) is highly variable. Nevertheless, as it has a larger number of objects than in our sample, we therefore use it to test the unified scheme hypothesis. We use Kukula et al. (1995) data and plot the distribution for Seyfert 1 galaxies (Seyfert 1.0, 1.5 and 1.8) and Seyfert 2 galaxies (Seyfert 1.9 and 2.0) to compare radio luminosities, projected linear sizes, and relativistic beaming. Note that, as per our definition, Seyfert 1 galaxy has Doppler widths of  $H\beta$  (or  $H\alpha$ ) emission lines greater than  $1000 \text{ km s}^{-1}$ , whereas Seyfert 1.9 and 2.0 do not (Seyfert 1.9 shows faint  $H\alpha$  and not  $H\beta$ ).

#### 3.7.1. Radio luminosity comparisons

Almost all the objects in this well defined sample were detected at radio wavelengths (39 of the 48 by VLA *A* array and

TABLE 6  
TABLE SHOWING SUMMARY OF THE  
CLASSIFICATION OF THE RADIO  
MORPHOLOGIES, AND THE NUMBER OF SOURCES  
SEEN ON THE TWO VLA CONFIGURATIONS FOR  
THE CfA SEYFERT GALAXY SAMPLE.

Morphology <sup>1,2,3</sup>	VLA <i>A</i> array	VLA <i>C</i> array
not detected	8	6
unresolved	17	20
slightly resolved	5	9
resolved	14	8
Compact double	1	1
no data	3	4

REFERENCES. — (1) Ulvestad & Wilson (1984A); (2)  
Ulvestad & Wilson (1984A); (3) Ulvestad & Ho (2001).

42 of the 48 by VLA *C* array), so it is valid to test for the distribution of total VLA *A* array and VLA *C* array radio luminosity. Figures 4A and 4B show the distributions of the total detected radio luminosities by VLA *A* array and by VLA *C* array configurations, respectively. It suggest that there is a decent similarity in the two distribution for Seyfert 1 and Seyfert 2 galaxies. We use the Mann-Whitney U test to test the hypothesis that the two distributions of total radio luminosities detected using VLA *A* configuration and VLA *C* configuration are similar. The results of this test indicate that the distribution of Seyfert 1 and Seyfert 2 galaxies are similar at a significance level of 0.15 for the CfA Seyfert sample using both VLA array configurations at 8.4 GHz. We also compare the distribution of the extended radio luminosity, corresponding to the difference of the flux density detected by the VLA *C* and VLA *A* array shown in Figure 4C. The Mann-Whitney U test gives a significance level of 0.20 that the distribution of Seyfert 1 and Seyfert 2 galaxies are same. This significance level is not high enough to demonstrate statistically that the distributions are the same, but it does not contradict the possibility that they are the same. We thus conclude that the distributions of the radio luminosity of Seyfert 1 and Seyfert 2 galaxies for the CfA Seyfert sample at 8.4 GHz are probably similar at all scales and is consistent with the predictions of the unified scheme.

#### 3.7.2. Projected linear sizes

Table 6 summarizes the classification of the radio morphology for the CfA Seyfert galaxy sample, following the scheme of Ulvestad & Wilson (1984B). The numbers in the corresponding columns in the Table shows the number of sources seen of the kinds mentioned in Ulvestad & Wilson (1984A,B) and Ulvestad & Ho (2001) on each VLA configuration. The Seyfert galaxy samples used for the comparison are (i) Markarian, based on ultraviolet-excess selection criteria containing 29 sources (Ulvestad & Wilson 1984A); (ii) distance-limited, heterogeneous selection criteria containing 57 sources (Ulvestad & Wilson 1984B, 1989); and (iii) Palomar, optical selection criteria containing 45 sources (Ho & Ulvestad 2001; Ulvestad & Ho 2001). As compared to Wilson (1991), Kukula et al.'s (1995) measurements show a higher fraction of unresolved sources and a lower fraction of galaxies with diffuse/linear radio emission. This result may be due to an observational bias; these observations are not as sensitive to diffuse, extended, steep spectrum emission as are the 20 cm VLA observations of Ulvestad & Wilson (1989).

We use angular sizes tabulated in Kukula et al.'s (1995) paper along with our formulation in Section 3.3 to determine the linear size and plot the distribution of linear sizes de-

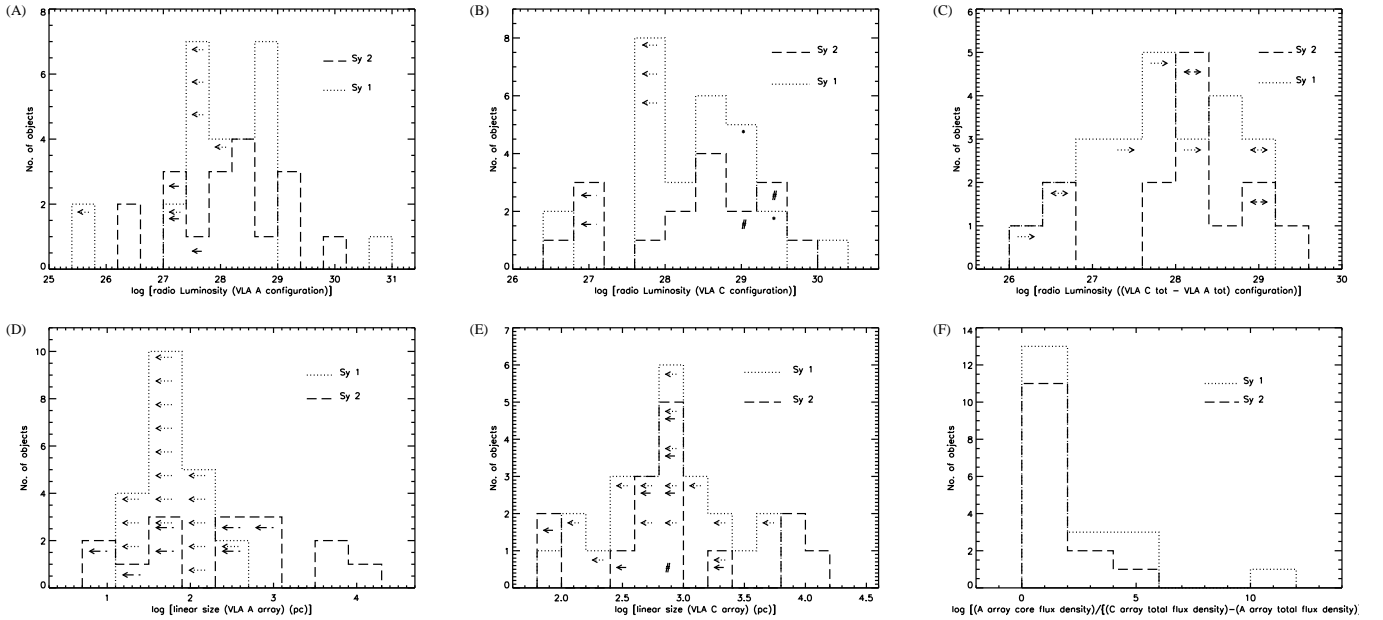


FIG. 4.— Histograms showing distributions of total detected radio luminosity ( $\text{ergs s}^{-1}\text{Hz}^{-1}$ ) for the CfA Seyfert sample at 8.4 GHz using VLA A array; arrows denote undetected objects (A), the radio luminosity ( $\text{ergs s}^{-1}\text{Hz}^{-1}$ ) for the CfA Seyfert sample at 8.4 GHz using VLA C array; ‘\*’ and ‘#’ denote an error of  $\sim 20\%$  in flux density calibration for Seyfert 1 and 2 galaxies respectively; arrows denote undetected objects (B), the total extended radio luminosity ( $\text{ergs s}^{-1}\text{Hz}^{-1}$ ) for the CfA Seyfert sample at 8.4 GHz; single-headed arrow indicates non-detection on VLA A configuration and double-headed arrow indicates non-detection on both the configurations (C), projected linear size (pc) of the source as measured by VLA A array for the CfA Seyfert galaxy sample at 8.4 GHz; arrows indicate unresolved objects (D), projected linear size (pc) of the source as measured by VLA C array for the CfA Seyfert galaxy sample at 8.4 GHz; ‘#’ for an object in a bin denotes the VLA A array linear size for it, and arrows indicate unresolved objects (E), and fraction of the radio core flux density detected by VLA A array as against the extended flux density,  $R$  for the CfA Seyfert sample at 8.4 GHz (F).

rived from VLA A array shown in Figure 4D and VLA C array shown in Figure 4E measurements for the two classes of Seyfert galaxies (arrows denote the upper limits to the sizes). The Mann-Whitney U tests show that the two distributions are statistically distinguishable at a significance level of 0.10 and 0.05 for the linear projected sizes of the two classes of the Seyfert galaxies on the basis of VLA C array and VLA A array measurements, respectively. We thus believe that Seyfert 2 galaxies tend to show larger projected linear sizes than Seyfert 1 galaxies when found using VLA A configuration and VLA C configuration, and this is consistent with the unified scheme. This is also consistent with the result obtained by Morganti et al. (1999).

### 3.7.3. Relativistic beaming

To investigate relativistic beaming, we use the distribution of the ratio between the possibly beamed and extended radio flux densities. We assume that the emission associated with the difference of the emissions between VLA C and VLA A configurations would not be Doppler boosted and we call this as an extended emission. The VLA A configuration measurement probes structures on scales smaller than VLA C configuration and we use VLA A configuration emission as the one which would suffer from Doppler boosting if beaming is present. Figure 4F shows the distribution of the ratio  $R$  (defined in Section 3.5), of the two, VLA A configuration emission to the extended emission as an indicator of relativistic beaming. The Mann-Whitney U test is not conclusive about whether the distributions are the same or not at a significance level of 0.25. Note that the two observations, VLA C and VLA A array for the CfA Seyfert sample, are not simultaneous as they were for our Seyfert sample, and we have discussed

earlier that Seyfert galaxies show radio variability. Furthermore, here the distribution of  $R$  and its statistical significance does not actually compare the flux density detected on pc-scales against the extended emission and hence is not really a measure of relativistic beaming. But nevertheless we use it as an indicator to probe the boosting of core flux density in Seyfert galaxies. Since it is equally likely that the distributions obtained here are either same or different, and considering also the results based on our Seyfert sample, we conclude that Seyfert galaxies do not show relativistic bulk motion in their nuclei.

## 4. CONCLUSIONS

Unification of Seyfert 1 and Seyfert 2 galaxies has been attempted by various authors in the past. Their radio emission has been extensively studied at  $\sim$  arcsec-scales, but at mas-scales a systematic study has not been done before. We carefully selected and made a list of 20 Seyfert galaxies that are matched in orientation-independent parameters which are measures of intrinsic AGN power and host galaxy properties. Additionally, the sample met the feasibility requirements, i.e., each sample source had a detectable compact core component at arcsec-scale resolution with flux density greater than 8 mJy at 5 GHz. This sample was used to test the unification scheme hypothesis rigorously by observing it at pc-scales. Although these results are based on a small sample size, these are valuable data for the faintest and least luminous radio cores of AGN using Global-VLBI.

Using our measured radio flux densities of the pc-scale and kpc-scale structures for Seyfert galaxies and their derived detection rates, radio luminosities, spectral indices, and projected linear sizes, we find that: (i) A starburst alone can-

not power these radio sources because, they have high brightness temperature, and the core radio luminosity at 5 GHz is  $\sim 10^{28}$  ergs s<sup>-1</sup>Hz<sup>-1</sup> and arises from a region smaller than a few cubic pc. (ii) Our sample of Seyfert 1 and Seyfert 2 galaxies have equal tendency to show compact radio structures, in contrast to the results of Roy et al. (1994), who concluded that compact radio structures were much more common in Seyfert 2 galaxies than in Seyfert 1 galaxies. (iii) The distributions of pc-scale and kpc-scale radio luminosities are similar for both Seyfert 1 and Seyfert 2 galaxies. This is consistent with the prediction of the unified scheme hypothesis. (iv) We do not find any evidence for relativistic beaming in Seyfert galaxies. (v) Although nuclei of Seyfert galaxies show a variation in their nuclear flux density (Mundell et al. 2009), our sample of Seyfert 1 and Seyfert 2 galaxies show similar distributions of source spectral indices. (vi) The unification scheme hypothesis predicts that Seyfert 1 galaxies oriented at small angles to the line of sight should have systematically smaller projected linear size than Seyfert 2 galaxies. The distributions for Seyfert 1 and Seyfert 2 galaxies of our sample are not significantly different as would be expected in the unified scheme. This could be mainly due to a relatively large spread in the intrinsic sizes.

Additionally, from the radio observations of the CfA Seyfert galaxy sample (Kukula et al. 1995) and the kpc-scale data from them, the radio luminosities, projected linear size, and the ratio of flux density detected on VLA A array configuration and the extended emission detected on VLA C array

configuration for the two classes of Seyfert galaxies are consistent with the unification scheme hypothesis.

We thank the anonymous referee for her/his prompt review of the manuscript and for useful and detailed comments that lead to significant improvement of the paper. DVL is grateful to L. Lanz for her grammatical corrections. This project was done with financial support from the Indo-Russian International Long Term Programme of the Department of Science and Technology, Government of India and the Russian Academy of Sciences. Financial support in the initial phase from the Indian National Science Academy exchange programme is also acknowledged. DVL acknowledges support from the Joint Institute for VLBI in Europe for a visit there. DG acknowledges support from the European Commission under TMR contract No. ECBFMGECT950012. The VLA and VLBA are operated by the National Radio Astronomy Observatory. The National Radio Astronomy Observatory is a facility of the National Science Foundation operated under cooperative agreement by Associated Universities, Inc. The European VLBI Network is a joint facility of European, Chinese and other radio astronomy institutes funded by their national research councils. This research has made use of NASA's Astrophysics Data System bibliographic services, the NASA/IPAC Extragalactic Database (NED) which is operated by the Jet Propulsion Laboratory, California Institute of Technology, under contract with NASA, and the SIMBAD database, operated by CDS, Strasbourg, France.

#### REFERENCES

- Antonucci, R.R.J., 1993, *ARA&A*, 31, 473.  
 Barvainis, R., & Lonsdale, C.J. 1998, *ApJ*, 115, 885.  
 Baum, S.A., O'Dea, C.P., Dallacassa, D., de Bruyn, A.G., & Pedlar, A. 1993, *ApJ*, 419, 553.  
 Bicknell, G.V., Dopita, M.A., Tsvetanov, Z.I., & Sutherland, R.S., 1998, *ApJ*, 495, 680.  
 Blandford, R.D., & Rees, M.J., 1978, *PhyS*, 17, 265.  
 Blandford, R.D., & Königl, A., 1979, *ApJ*, 232, 34.  
 Brunthaler, A., Falcke, H., Bower, G.C., Aller, M.F., Aller, H.D., Terasranta, H., Lobanov, A.P., Krichbaum, T.P., & Patnaik, A.R., 2000, *A&AL*, 357, L45.  
 Buchanan, C.L., Gallimore, J.F., O'Dea, C.P., Baum, S.A.; Axon, D.J., Robinson, A., Elitzur, M., Elvis, M., 2006, *AJ*, 132, 401  
 de Bruyn, A.G., & Wilson, A.S. 1976, *A&A*, 53, 93.  
 Cappi, M., Mihara, T., Matsuoka, M., Brinkmann, W., Prieto, M.A., & Palumbo, G.G.C., 1996, *ApJ*, 456, 141.  
 Cid Fernandes, & Terlevich, R., 1995, *MNRAS*, 272, 423.  
 Cid Fernandes, Heckman T., Schmitt H., González Delgado R. M., Storchi-Bergmann T., 2001, *ApJ*, 558, 81.  
 Cid Fernandes, Gu Q., Melnick J., Terlevich E., Terlevich R., Kunth D., Rodrigues Lacerda R., & Jouguet B., 2004, *MNRAS*, 355, 273.  
 Colina, L., Vargas, M.L.G., Rosa M. Gonzalez, Mas-Hesse, J.M., Perez, E., Alberdi, A., & Krabbe, A., 1997, *ApJL*, 488, L71.  
 Condon, J.J., 1992, *ARA&A*, 30, 575.  
 Condon, J.J., Cotton, W.D., Greisen, E.W., Yin, Q.F., Perley, R.A., Taylor, G.B., & Broderick, J.J., 1998, *AJ*, 115, 1693.  
 Curran, S.J., 2000, *A&AS*, 144, 271.  
 Dahari, O., & De Robertis, M.M. 1988, *ApJS*, 67, 249.  
 Davis, M., Huchra, J., & Latham, D., in *Early evolution of universe and its present structure*, eds. Abell, G.O., & Chincarni, G., 1983, *IAUS*, 104, p. 167, Reidel, Dordrecht.  
 Dultzin-Hacyan, D., Krongold, Y., Fuentes-Guridi, I., & Marziani, P., 1999, *ApJ*, 513, L111.  
 Edelson, R.A. 1987, *ApJ*, 313, 651.  
 Evans, I.N., Ford, H.C., Kinney, A.L., Antonucci, A.J., Armus, L., & Caganoff, S. 1991A, *ApJL*, 369, L27.  
 Evans, I.N., Ford, H.C., Kinney, A.L., Antonucci, R.R.J., Armus, L., & Caganoff, S. 1991B, *ApJS*, 76, 985.  
 Evans, I.N., Tsvetanov, Z., Kriss, G.A., Ford, H.C., Caganoff, S., & Koratkar, A.P., 1993, *ApJ*, 417, 82.  
 Evans, I.N., Ford, H.C., Kriss, G.A., & Tsvetanov, Z., in *First Stromlo Symposium: The physics of active galaxies*, eds Bicknell, G.V., Dopita, M.A., & Quinn, P.J., 1994, *ASP Conf. Ser.*, 54, p. 3.  
 Falcke, H., Wilson, A.S., & Simpson, C. 1998, *ApJ*, 502, 199.  
 Falcke, H., Nagar, N.M., Wilson, A.S., & Ulvestad, J.S. 2000, *ApJ*, 542, 197.  
 Gallimore, J.F., Yzaguirre, A., Jakobski, J., Stevenosky, M.J., Axon, D.J., Baum, S.A., Buchanan, C.L., Elitzur, M., Elvis, M., O'Dea, C.P., & Robinson, A., 2010, *ApJS*, 187, 172.  
 González-Delgado, Rosa M., Heckman, T., Leitherer, C., Meurer, G., Krolik, J., Wilson, A.S., Kinney, A., Koratkar, A., 1998, *ApJ*, 505, 174.  
 González-Delgado, R.M., Heckman, T., & Leitherer, C., 2001, *ApJ*, 546, 845.  
 Goodrich, R.W., 1989, *ApJ*, 340, 190.  
 Heckman, T.M., in *Paired and Interacting Galaxies*, eds Sulentic, J.W., Keel, W.C., & Telesco, C.M. 1990A, *IAUC*, 124, p. 359, NASA.  
 Heckman, T.M., in *Massive stars in starbursts*, eds Walborn, N., & Leitherer, C., 1990B, *Proc. of the ST ScI symposium*.  
 Heckman, T.M., Gonzalez-Delgado, R., Leitherer, C., Meurer, G. R., Krolik, J., Wilson, A. S., Koratkar, A., & Kinney, A., 1997, *ApJ*, 482, 114.  
 Heckman, T.M., Sembach, K.R., Meurer, G.R., Leitherer, C., Calzetti, D., & Martin, C.L., 2001, *ApJ*, 558, 56.  
 Ho, L.C., Filippenko, A.V., & Sargent, W.L.W., 1996, *ApJ*, 462, 183.  
 Ho, L.C., Filippenko, A.V., Sargent, W.L.W., Peng, C.Y., 1997, *ApJS*, 112, 391.  
 Ho, L.C., & Ulvestad, J.S., 2001, *ApJS*, 133, 77.  
 Huchra, J., Davis, M., Latham, D., & Torny, J., 1983, *ApJS*, 52, 89.  
 Huchra, J., & Burg, R., 1992, *ApJ*, 393, 90.  
 Hunt, L.K., & Malkan, M.A., 1999, *ApJ*, 516, 660.  
 Johnston, K.J., Elvis, M., Kjer, D., & Shen, B.S.P. 1982, *ApJ*, 262, 61.  
 Kapahi, V.K., & Saikia, D.J., 1982, *JApA*, 3, 465.  
 Kauffmann, G. et al. 2003A, *MNRAS*, 341, 33.  
 Kauffmann, G. et al. 2003B, *MNRAS*, 341, 54.  
 Kellermann, K.I., Sramek, R., Schmidt, M., Shaffer, D.B., & Green, R. 1989, *AJ*, 98, 1195.  
 Keel, W.C., 1983, *ApJS*, 52, 229.  
 Khachikian, E.Y., & Weedman, D.W. 1974 *ApJ*, 192, 581.

- Kinney, A.L., Antonucci, R.R.J., Ward, M.J., Wilson, A.S., & Whittle, M., 1991, *ApJ*, 377, 100.
- Kim, D.-C., Veilleux, S., & Sanders, D.B., 1998, *ApJ*, 508, 627.
- Kriss, G.A., Tsvetanov, Z., & Davidsen, A.F., in *First Stromlo Symposium: The phy of active galaxies*, eds. Bicknell, G.V., Dopita, M.A., & Quinn, P.J., 1994, *ASP Conf. Ser.*, 54, p. 281.
- Krongold, Y., Dultzin-Hacyan, D., & Marziani, P., 2002, *ApJ*, 572, 169.
- Krolik, J.H. *Active Galactic Nuclei*, 1999, Princeton University Press.
- Kukula, M.J., Pedlar, A., Baum, S.A., & O'Dea, C.P. 1995, *MNRAS*, 276, 1262.
- Lal, D.V., Shastri, P., & Gabuzda, D.C., 2004, *A&A*, 425, 99.
- Lal, D.V. 2002, PhD Thesis, *Seyfert Galaxies: Nuclear Radio Structure and Unification*.
- Lawrence, A., & Elvis, M., 1982, *ApJ*, 256, 706.
- Lawrence, A., 1987, *PASP*, 99, 309.
- Lawrence, A., & Elvis, M., 2010, *ApJ*, 714, 561.
- Levenson, N.A., Weaver, K.A., & Heckman, T.M. 2001, *ApJ*, 550, 230.
- Lipovetsky, V.A., Neizvestny, S.I., & Neizvestny, O.M. 1988, *Soobshch. Spets. Astrofiz. Obs.*, 55, 5.
- Maiolino, R., Ruiz, M., Rieke, G.H., & Papadopoulos, P., 1997, *ApJ*, 485, 552.
- Mulchaey, J.S., Wilson, A.S., & Tsvetanov, Z. 1996, *ApJ*, 467, 197.
- Malkan, M.A., Gorjian, V., & Tam, R. 1998, *ApJS*, 117, 25.
- Muñoz Marín V.M., González Delgado R.M., Schmitt H.R., Cid Fernandes R., Pérez E., Storchi-Bergmann T., Heckman T., & Leitherer C., 2007, *AJ*, 134, 648.
- Markarian, B.E., *Astrophysics*, 1967, 3, 24.
- Markarian, B.E., Stepanian, J.A., & Erastova, L.K., 1986, *Astronomy*, 25, 345.
- Mas-Hesse, J.M., Rodríguez-Pascual, P.M., de Córdoba, L.S.F., Mirabel, I.F., 1994, *ApJS*, 92, 599.
- Meurs, E.J.A., & Wilson, A.S., 1984, *A&A*, 136, 206.
- Miller, J.S., & Goodrich, R.W., 1990, *ApJ*, 355, 456.
- Morganti, R., Tsvetanov, Z.I., Gallimore, J., & Allen, M.G., 1999, *A&AS*, 137, 457.
- Mundell, C.G., Wilson, A.S., Ulvestad, J.S., & Roy, A.L. 2000, *ApJ*, 529, 816.
- Mundell, C.G., Ferruit, P., Nagar, N. Wilson, A.S., 2009, *ApJ*, 703, 802.
- Muxlow, T.W.B., T.W.B., Pedlar, A., Wilkinson, P.M., Axon, D.J., Sanders, E.M., & de Bruyn, A.G., 1994 *MNRAS*, 266, 455.
- Nagar, N.M., & Wilson, A.S. 1999, *ApJ*, 516, 79.
- Nagar, N.M., Wilson, A.S., Mulchaey, J.S., & Gallimore, J.F. 1999, *ApJS*, 120, 209.
- Nagar, N.M., Falcke, H., Wilson, A.S., & Ho, L.C. 2000, *ApJ*, 542, 186.
- Nelson, C.H., & Whittle, M. 1995, *ApJS*, 99, 67.
- Nelson, C.H., & Whittle, M., 1996, *ApJ*, 465, 96.
- Norris, R.P., Kesteven, M.J., Wellington, K.J., & Batti, M.J., 1988, *ApJS*, 67, 85.
- Norris, R.P., Roy, A.L., Allen, D.A., Kesteven, M.J., Troup, E.R., & Reynolds, J.E., in *Relationships between active galactic nuclei and starburst galaxies*, ed. Filippenko, A.V. 1992A, *ASP Conf Series*, 31, p. 71.
- Norris, R.P., Kesteven, M.J., & Calabretta, M.R., 1992B, *Jl. Elect. of Elec. and Engg.*, Austr., 12, 205.
- Osterbrock, D.E., 1981, *ApJ*, 249, 462.
- Osterbrock, D.E., & Pogge, R.W., 1985, *ApJ*, 297, 166.
- Pedlar, A., Kukula, M.J., Longley, D.P.T., Muxlow, T.W.B., Axon, D.J., Baum, S.A., O'Dea, C.P., & Unger, S.W., 1993, *MNRAS*, 263, 471.
- Penessa, F., Bassani, L., 2002, *A&A*, 394, 435.
- Parra, R., Conway, J.E., Diamond, P.J., Thrall, H., Lonsdale, C.J., Lonsdale, C.J., & Smith, H.E., 2007, *ApJ*, 659, 314
- Peterson, B.M. *An introduction to the Active Galactic Nuclei*, 1997, Cambridge University Press.
- Pogge, R.W. 1989, *ApJS*, 71, 433.
- Pringle, J.E., Antonucci, R.R.J., Clarke, C.J., Kinney, A.L., Schmitt, H.R., & Ulvestad, J.S. 1999, *ApJL*, 526, L9.
- Raimann, D., Storchi-Bergmann, T., González Delgado, R.M., Cid Fernandes, R., Heckman, T., Leitherer, C., Schmitt, H.R., 2003, *MNRAS*, 339, 772.
- Roy, A.L., Norris, R.P., Kesteven, M.J., Troup, E.R., & Reynolds, J.E. 1994, *ApJ*, 432, 496.
- Rupen, M.P., van Gorkom, J.H., Knapp, G.R., Gunn, J.E., & Schneider, D.P., 1987, *AJ*, 94, 61.
- Sandage, A.R., in *Galaxies and the Universe*, eds. Sandage, A.R., Sandage, M., Kristian, J., *Stars and Stellar Systems*, 1975, 9, p.1, Univ. Chicago.
- Schmidt, M., & Green, R.F. 1983, *ApJ*, 269, 352.
- Schmitt, H.R., Storchi-Bergmann, T., Cid Fernandes, R., 1999, *MNRAS*, 303, 173.
- Schmitt, H.R., Ulvestad, J.S., Antonucci, R.R.J., & Kinney, A.L. 2001, *ApJS*, 132, 199.
- Shuder, J.M. 1981, *ApJ*, 244, 12.
- Siegel, S., & Castellan Jr., N.J. 1981, *Nonparametric Statistics for the Behavioral Sciences*.
- Smith, H.E., Lonsdale, C.J., Lonsdale, C.J., Diamond, P.J., 1998, *ApJL*, 493, L17.
- Smith, H.E., Lonsdale, C.J., & Lonsdale, C.J. 1998, *ApJ*, 492, 137.
- Storchi-Bergmann T., Raimann D., Bica E. L.D., & Fraquelli H.A., 2000, *ApJ*, 544, 747.
- Storchi-Bergmann T., González Delgado, R.M., Schmitt, H.R., Cid Fernandes, R., & Heckman, T., 2001, *ApJ*, 559, 147.
- Su, B.M., Muxlow, T.W.B., Pedlar, A., Holloway, A.J., Steffen, W., Kukula, M.J., & Mutel, R.L. 1996, *MNRAS*, 279, 1111.
- Terlevich, R., in *Windows on galaxies*, eds. Fabbiano, G., Gallagher, J. & Renzini, A., 1990A, *ASSL*, p. 87, Kluwer: Dordrecht.
- Terlevich, R., in *Structure and dynamics of the inter-stellar medium*, eds. Tenorio-Tagle, G., Moles, M., & Melnick, J., 1990B, p. 343, Springer-Verlag: Berlin.
- Terlevich, R. & Boyle, B.J., 1993, *MNRAS*, 262, 491.
- Thean, A., Pedlar, A., Kukula, M.J., Baum, S.A., & O'Dea, C.P. 2001, *MNRAS*, 325, 737.
- Tran, H.D., 2001, *ApJ*, 554, L19.
- Tran, H.D., 2003, *ApJ*, 583, 632.
- Ulvestad, J.S., Wilson, A.S., & Sramek, R.A., 1981, *ApJ*, 247, 419.
- Ulvestad, J.S., 1982, *ApJ*, 259, 96.
- Ulvestad, J.S., & Wilson, A.S. 1984A, *ApJ*, 278, 544.
- Ulvestad, J.S., & Wilson, A.S. 1984B, *ApJ*, 285, 439.
- Ulvestad, J.S. 1986, *ApJ*, 310, 136.
- Ulvestad, J.S., & Wilson, A.S. 1986, *MNRAS*, 218, 711.
- Ulvestad, J.S., & Wilson, A.S. 1989, *ApJ*, 343, 659.
- Ulvestad, J.S., & Antonucci, R.R.J., Goodrich, R.W. 1995, *AJ*, 109, 81.
- Ulvestad, J.S., Roy, A.L., Colbert, J.M., & Wilson, A.S. 1998, *ApJ*, 496, 196.
- Ulvestad, J.S., Wrobel, J.M., & Carilli, C.L. 1999A, *ApJ*, 516, 127.
- Ulvestad, J.S., Wrobel, J.M., Roy, A.L., Wilson, A.S., Falcke, H., & Krichbaum, T.P. 1999B, *ApJL*, 517, L81.
- Ulvestad, J.S., 1999, *VLBA operations memo No. 34*, NRAO.
- Ulvestad, J.S., 2000, *VLBA scientific memo No. 25*, NRAO.
- Ulvestad, J.S., & Ho, L.C. 2001, *ApJ*, 558, 561.
- Unger, S.W., Pedlar, A., Neff, S.G., & de Bruyn, A.G. 1984, *MNRAS*, 209, 15P.
- Unger, S.W., Pedlar, A., Booler, R.V., & Harrison, B.A. 1986, *MNRAS*, 219, 387.
- Urry, C.M., & Padovani, P. 1995, *PASP*, 107, 803.
- de Vaucouleurs, G., de Vaucouleurs, A., Corwin (Jr.) H.G., Buta, R.J., Paturel, G., & Fouque, P. *Third reference catalogue of bright galaxies (RC3)*, version 3.9, 1991, Springer-Verlag, New York.
- Veron, P., in *Structure and evolution of active galactic nuclei*, eds. Giuricin, G., Mardirossian, F., Mezzetti, M., & Ramella, M. 1986, *ASSL*, p. 253, D. Reidel Publishing Co.
- Weedman, D.W. 1977, *ARA&A*, 15, 69.
- Whittle, M., Pedlar, A., Meurs, E.J.A., Unger, S.W., Axon, D.J., Ward, M.J., 1988, *ApJ*, 326, 125.
- Whittle, M. 1992A, *ApJS*, 79, 49.
- Whittle, M., 1992B, *ApJ*, 387, 109.
- Whittle, M., 1992C, *ApJ*, 387, 121.
- Wilson, A.S. & Ulvestad, J.S., 1982, *ApJ*, 263, 576.
- Wilson, A.S. & Ulvestad, J.S., 1983, *ApJ*, 275, 8.
- Wilson, A.S., Baldwin, J.A., Sun, Sze-Dung, & Wright, A.E., 1986, *ApJ*, 310, 121.
- Wilson, A.S. & Keel, W.C. 1989, *AJ*, 98, 1581.
- Wilson, A.S., Helfer, T.T., Haniff, C.A., & Ward, M.J. 1991, 381, 79.
- Wilson, A.S., in *The interpretation of modern synthesis observations of spiral galaxies*, eds. Duric, N., & Crane, P.C. 1991, *ASP*, 18, p. 227.
- Wrobel, J.M. 1995, "VLBI observing strategies", in *Very Long Baseline Interferometry and the VLBA*, eds. Zensus, J.A., Diamond, P.J., & Napier, P.J. 1995, *ASP Conf Series*, 82, p. 411.
- Wrobel, J.M. *VLBA observational status summary*, 2000A, NRAO.
- Yee, H.K.C. 1980, *ApJ*, 241, 894.